Available online at www.sciencedirect.com

ScienceDirect

Surface Science Reports 70 (2015) 424–447

surface science reports

www.elsevier.com/locate/surfrep

Atomistic details of oxide surfaces and surface oxidation: the example of copper and its oxides

Chiara Gattinoni, Angelos Michaelides*

Thomas Young Centre, London Centre for Nanotechnology and Department of Chemistry, University College London, 17-19 Gordon Street, London WC1H 0AH, UK

Received 20 May 2015; received in revised form 7 July 2015; accepted 14 July 2015
Editor: Ulrike Diebold

Abstract

The oxidation and corrosion of metals are fundamental problems in materials science and technology that have been studied using a large variety of experimental and computational techniques. Here we review some of the recent studies that have led to significant advances in our atomic-level understanding of copper oxide, one of the most studied and best understood metal oxides. We show that a good atomistic understanding of the physical characteristics of cuprous (Cu_2O) and cupric (CuO) oxide and of some key processes of their formation has been obtained. Indeed, the growth of the oxide has been shown to be epitaxial with the surface and to proceed, in most cases, through the formation of oxide nano-islands which, with continuous oxygen exposure, grow and eventually coalesce. We also show how electronic structure calculations have become increasingly useful in helping to characterise the structures and energetics of various Cu oxide surfaces. However a number of challenges remain. For example, it is not clear under which conditions the oxidation of copper in air at room temperature (known as native oxidation) leads to the formation of a cuprous oxide film only, or also of a cupric overlayer. Moreover, the atomistic details of the nucleation of the oxide islands are still unknown. We close our review with a brief perspective on future work and discuss how recent advances in experimental techniques, bringing greater temporal and spatial resolution, along with improvements in the accuracy, realism and timescales achievable with computational approaches make it possible for these questions to be answered in the near future.

Contents

*Corresponding author.
E-mail addresses: c.gattinoni@ucl.ac.uk (C. Gattinoni), angelos.michaelides@ucl.ac.uk (A. Michaelides).

http://dx.doi.org/10.1016/j.surfrep.2015.07.001
0167-5729/

1. Introduction

Copper is a material which has accompanied human prehistory and history, and it is still highly relevant today. Cold working of copper has been performed for at least 10,000 years and smelting of copper ore for around 7000 years [1]. Its use as a construction material, *e.g.* in piping, can be dated back to ancient Egypt, and its importance in this field has not diminished nowadays. In the modern world it has acquired further uses, for example in electrical systems and electronic devices.

Within this long history, the properties of copper have been extensively studied and exploited, however much is still unknown about this important metal. In particular, the oxidation and corrosion of copper, which impacts its performance in industrial and technological applications, is still not completely understood.

Copper is found to readily oxidise at room temperature [2–4], and the presence of an oxide layer, however thin, can compromise its uses in technology. As an example, copper could be an environmentally friendly and low-cost substitute for the (currently used) tin-lead or (promising) gold- and silver-based solder alloys in electronic packaging, if there was a way to prevent its oxidation [5]. Moreover, copper canisters are used for nuclear waste disposal, and understanding the oxidation and corrosion of copper in anaerobic conditions is thus of critical importance [6]. On the other hand, the existence of stable copper oxides at room temperature, with a ~ 2.0 eV band gap, makes them interesting for catalytic [7], gas sensing [8], optoelectronic and solar technologies [9,10]. Thus, there currently is a two-fold interest in understanding copper oxides: from the one hand, to mitigate against technological failure, and on the other hand, to exploit their potential industrial applications.

Copper is also considered a model system to understand the formation of metal oxides in general. The atomistic details of the oxidation process tend to be system-specific, with some metals showing uniform oxide growth (*e.g.* Ref. [11]), and others complex temperature-dependent phenomena such as surface roughening (*e.g.* Ref. [12]) and island formation (*e.g.* Refs. [13,14]). However, the copper oxidation process is one of the most studied with a large number of experimental and computational methods, and one of the better understood. Therefore, a detailed understanding of copper oxidation, of the techniques used to study it and of the challenges which are still open is invaluable when considering the oxidation process on any other system.

In this review, we discuss the status of knowledge of copper oxidation from the atomistic point of view, which we believe is of key importance if we want to learn how to prevent or manipulate copper oxidation. We cannot hope to provide a complete review of all the work done on this subject since the beginning of the last century [15–17]. We are therefore going to focus on recent surface science, spectroscopy and atomistic computational work which has been performed to understand the properties of copper oxides and their formation, and on the open challenges that can be addressed using these techniques.

First, a brief overview on the experimental and computational techniques which have been used for the study of oxide structures and oxidation kinetics is given (Section 2), in order to clarify some of the terminology used throughout the review. The structural and electronic characteristics of the bulk oxides and their surfaces are then presented (Section 3). We subsequently look at the interaction of clean copper surfaces with oxygen and the initial stages of controlled oxidation (Section 4) as well as long-term oxidation (Section 5). Finally, in Section 6, conclusions and perspectives are given.

We hope that it will be clear from the following that tremendous progress has been made in understanding the atomistic details of copper oxides and their formation under different conditions. However, equally important gaps in our understanding remain, especially in terms of the formation kinetics and the structure of the resulting oxide surfaces.

2. Experimental and computational techniques

An enormous number of experimental [18–21] and computational techniques are available to investigate the physical and chemical characteristics of solids, surfaces and surface kinetic processes. Many of them have been used over the years to *e.g.*, understand oxide structures, characterise oxide surfaces, understand the oxidation kinetics and investigate bulk properties of the oxides. For clarity, in this section we provide a brief introduction to the most relevant techniques which have been used on copper oxide and which are going to be mentioned in the following sections, with an emphasis on strengths and weaknesses of each approach.

In early studies of oxidation, thermogravimetric analysis (TGA), where changes in physical and chemical properties of materials are measured as a function of time, was widely used to study the onset of oxidation by recording the mass gain of a sample under oxygen exposure. Whilst useful in providing a

broad overview of the extent of oxidation, this technique is however unable to provide atom-resolved information.

Imaging techniques such as electron microscopy (EM), transmission electron microscopy (TEM) and their derivatives (*e.g.*, high-resolution transmission electron microscopy (HRTEM) or field emission scanning electron microscopy (FESEM)) and surface-specific techniques such as scanning tunnelling microscopy (STM) can be applied to surfaces and provide atomistic level structural information. As we will see, they have been amply used to image adsorption of oxygen on the copper surface, surface reconstructions and initial oxide formation. The atomic composition and oxidation states of the atoms in a material can be obtained using spectroscopic techniques such as X-ray diffraction (XRD), Auger electron spectroscopy (AES), electron energy loss spectroscopy (EELS), low-energy electron diffraction (LEED), reflection high-energy electron diffraction (RHEED), X-ray photoelectron spectroscopy (XPS or ESCA) and X-ray absorption spectroscopy (XAS). The space- and time-resolution of these techniques has greatly improved since they were first used in this field (in the 1980s), as well as their range of applicability: for example, experiments at relatively high pressures can be performed nowadays [22].

Growth of the oxide and its atomic composition has been extensively studied by means of ellipsometry. This technique measures changes in polarisation as light interacts with an object and the resulting data are fitted with a 'guess' model for the material.

Computer simulations have also been widely applied to study the structural, optical and vibrational characteristics of copper oxides. When carrying out simulations of materials at the atomic scale, classical empirical potentials (force fields) or more sophisticated quantum (*ab initio*) approaches, such as density functional theory (DFT), can be used. Force fields are parametrised empirical potentials tuned to reproduce the interactions of the atoms in the system at hand. For certain problems force fields can provide a faithful description. However, the reliability and transferability of such calculations depends primarily on the extent and quality of the data used in their construction. Moreover, force fields cannot generally be applied to study chemical reactions. Current development in force fields are addressing these issues. Indeed, parametrisations obtained by fitting large data sets using *e.g.*, neural network [23] and machine learning methods [24], to name just two, are improving accuracy and transferability. Moreover, bond order potentials (such as ReaxFF [25]) and polarisable force fields [26] are making it possible to simulate chemical reactions. It is difficult to make general statements about the sizes of systems that can be explored with various methods. However, with many standard force fields it is now possible to examine systems with $\sim 100,000$ atoms on a routine basis. In addition, it is possible to explore the evolution of a system of this size, again on a routine basis, with an approach such as molecular dynamics for several hundreds of nanoseconds.

More accurate approaches are *ab initio* methods which aim to study the structure and properties of a material by seeking (approximate) solutions to very complex quantum mechanical equations such as the many-body Schrödinger equation. These methods are more general and do not require system-specific parametrisations, however they are computationally more expensive. One of the most widely used methods to study the properties of bulk materials and surfaces is density functional theory (DFT) [27–30]. With DFT it is possible to make genuine predictions about structural properties of a material within a few percent of the experimental value. DFT also provides access to the electronic structure of the systems being considered and related spectroscopic properties. In DFT, the energy of the electronic system is determined from the electronic density by solving Schrödinger-like equations. Whilst exact in principle, in practice approximations have to be introduced since the functional form of the electron–electron interaction, called the exchange-correlation (XC) functional, is unknown. Many approximate XC functionals have been developed [31], the most common ones being the local density approximation (LDA) and the generalised gradient approximation (GGA). A number of deficiencies in DFT arise from these approximations and the choice of an appropriate XC functional is critical in order to obtain meaningful results. As an example, in strongly correlated systems like CuO (typically, where *d* and *f* orbitals are localised), the GGA and LDA functionals provide a poor description of the electronic and bulk crystal structure. Moreover, the band gap obtained using GGA or LDA in semiconductors or insulators is generally underestimated. In these cases it is possible to add simple but somewhat *ad hoc* corrections to the functionals (*e.g.* the Hubbard *U* [32], self-interaction correction SIC [33]) or to use more sophisticated hybrid functionals (*e.g.* HSE06 [34], PBE0 [35]) which incorporate some exact Hartree–Fock exchange. Compared to standard empirical potential methods, DFT is much more computationally demanding, and, on a routine basis, systems with only a few 100 atoms can be examined and the dynamics of such systems explored for only a few tens of picoseconds.

Other computational methods which have been used in copper oxide simulations are the GW method [36], used when optoelectronic properties are of interest, since it is more accurate at predicting band structures than standard DFT XC functionals. In addition there have been a number of Hartree–Fock [37] studies and calculations with simpler approaches, such as the linear combination of atomic orbitals (LCAO) and tight binding methods [38].

3. Oxide structures

We are going to introduce here the bulk and surface structures of the two main copper oxides, Cu_2O and CuO. Knowledge of the physical properties of these materials, and especially of the surface structures, is relevant background when trying to understand the formation and growth of the copper oxide.

The two most common forms of the oxide (shown in Fig. 1) are cuprite (or cuprous oxide, Cu_2O), the principal oxide at low temperatures and pressure, and tenorite (or cupric oxide, CuO), dominant at high temperatures and pressures [39]. Another copper oxide structure, paramelaconite (Cu_4O_3), exists as a rare mineral found in hydrothermal deposits of copper. Cuprite has long been known to be the primary oxide for copper at

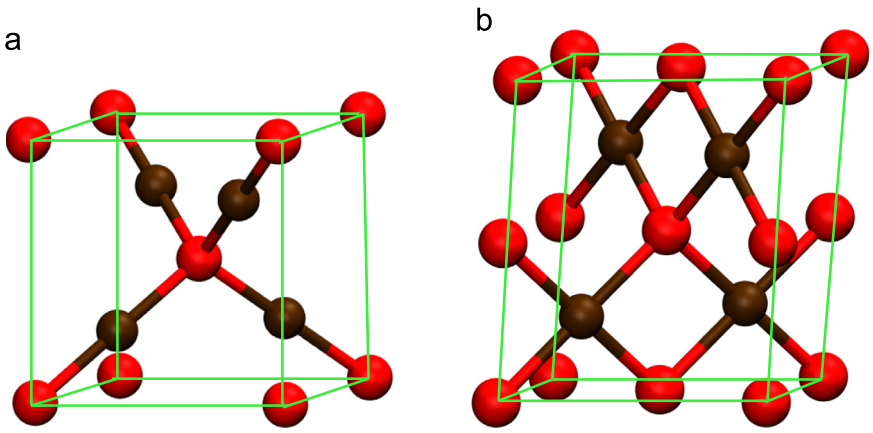

Fig. 1. Ball-and-stick model of a unit cell of (a) cuprous oxide Cu_2O and (b) cupric oxide CuO. Red balls represent oxygen and brown balls copper. The unit cell is shown in green. (For interpretation of the references to colour in this figure caption, the reader is referred to the web version of this paper.)

ambient conditions and there is considerable interest in its application to catalysis, optoelectronics and gas sensing and therefore a large amount of work has been done to determine its physical and chemical characteristics. Tenorite has been studied less and still relatively little is understood about the structure of its surfaces, with only a handful of experimental and computational studies performed to that aim.

3.1. Cu_2O bulk properties

In cuprous oxide (Cu_2O, see Fig. 1a), a cubic crystalline solid, copper has a Cu^{1+} oxidation state. It is a *p*-type semiconductor with a direct band gap of 2.02–2.17 eV and an optical gap of 2.62 eV [40,10,41]. It is a promising material for a variety of industrial applications because of its band gap and because it shows negative thermal expansion [42,43].

The properties of cuprous oxide have been extensively studied using empirical potentials [44], tight binding [45] and *ab initio* methods. *Ab initio* studies include the use of DFT methods (see Table 1), and good agreement with the experimental bulk structure (*i.e.* no more than 2.5% discrepancy between the calculated and the experimental value of the lattice constant) and vibrational modes [46] have been found. However, the band gap is underestimated with standard DFT XC functionals, yielding values between 0.5 and 0.8 eV [47–49] and grossly overestimated with Hartree–Fock at 9.7 eV [50]. Corrections to DFT (*e.g.* DFT + U or the GW approximation applied to DFT-GGA) give rise to band gaps that are in better agreement with experiment [51–56], as summarised in Table 1.

3.2. Cu_2O surfaces

Experimental data are available only for the $Cu_2O(100)$ and $Cu_2O(111)$ low index surfaces of cuprous oxide, by means of XPS (which provides information on the Cu to O ratio on the surface), LEED in ultra high vacuum (which identifies the periodicity of the surface), and in the case of $Cu_2O(111)$, also with TEM.

We first consider the polar $Cu_2O(100)$ surface, which is formed by a succession of purely Cu or O layers and yields bulk-truncated surfaces which are either O- or Cu-terminated (Fig. 2a). Polar surfaces generally reconstruct [69] and three different reconstructions were observed on $Cu_2O(100)$ according to the preparation method [70]. The most stable surface in vacuum is a Cu-terminated surface with a $(3\sqrt{2} \times \sqrt{2})R45^\circ$ reconstruction. The LEED pattern (which however showed many missing spots and the reconstruction is presented as tentative) was interpreted as a relaxation of the top layer of copper cations forming two surface dimers (d1 and d2 in Fig. 2a). Two transient structures were also identified: at 900 K, a $(\sqrt{2} \times \sqrt{2})R45^\circ$ reconstruction presenting a 1/2 layer of terminal oxygen, and, after long oxygen exposures, the stoichiometric (1×1) O-terminated surface. Both structures revert to the $(3\sqrt{2} \times \sqrt{2})R45^\circ$ reconstruction upon further annealing over 500 K. The $(3\sqrt{2} \times \sqrt{2})R45^\circ$ reconstruction has been reproduced computationally [71], and it is more stable than the Cu- or O-terminated $(\sqrt{2} \times \sqrt{2})R45^\circ$ reconstruction [72,73,63].

The other experimentally studied surface is $Cu_2O(111)$. A $Cu_2O(111)$ slab is formed by a succession of O–Cu–O trilayers, ending with either a (stoichiometric, non-polar) oxygen or (non-stoichiometric) copper termination (Fig. 2b). Photoemission and LEED experiments on this Cu-terminated (111) surface found, after annealing in UHV, a nearly stoichiometric reconstruction, with $(\sqrt{3} \times \sqrt{3})R30^\circ$ periodicity, attributed to an ordered 1/3 of an atomic layer of oxygen vacancies [70,54]. Conversely, annealing in oxygen gives a stoichiometric oxygen-terminated surface (with possibly the loss of the unsaturated copper atoms, Cu_{cus} in Fig. 2b, at the centre of the hexagons) [54]. The stability of both polar and non-polar stoichiometric $Cu_2O(111)$ surfaces has been studied also computationally [47,74–78] by means of DFT combined with, in some cases, *ab initio* thermodynamics. *Ab initio* thermodynamics (see *e.g.* [79,80]) is a technique which allows one to estimate relative system stabilities in different environments; in this case, the stability of different oxide surfaces at a range of temperatures and oxygen partial pressures. These studies showed that the experimentally observed $Cu_2O(111)$ surfaces are indeed the most stable. [76].

Table 1
Summary of the calculated lattice constant a, bulk modulus B and band gap for Cu_2O. Information on the exchange-correlation (XC) functional is also given. PBE is a GGA functional. scGW, G_0W_0 and GW+V_d are different applications of the GW method. HF+LYP is a Hartree–Fock type calculation with an *a posteriori* correction using the LYP correlation functional. For calculations using the $+U$ Hubbard correction, reported values of the relevant parameters used ($U-J$) are given in eV units. The experimental range of bulk moduli is due to different experimental techniques and fitting methodologies.

Ref.	a (Å)	B (GPa)	Band gap (eV)	XC
Cortona [57]	4.22	141	–	LDA
Filippetti [53]	4.23	–	0.55	LDA
Gordienko [58]	4.27	–	2.87	LDA
Nie [59]	4.22	–	0.52	LDA
Heinemann [60]	4.17	–	0.99	LDA+U ($U-J$=6.52)
Tran [61]	4.27[a]	–	0.63–0.94	LDA+U ($3<U-J<11$)
Cortona [57]	4.36	106	–	PBE
Islam [47]	4.31	–	0.7	PBE
Isseroff [62]	4.18	145	0.68	LDA
Isseroff [62]	4.10–4.17	135–143	0.81–1.15	LDA+U ($2<U-J<8$)
Isseroff [62]	4.31	109	0.43	GGA
Isseroff [62]	4.26–4.30	96–106	0.54–0.84	GGA+U ($2<U-J<8$)
Isseroff [62]	4.28	114	2.84	PBE0
Isseroff [62]	4.29	114	2.04	HSE
Le [63]	4.317	–	–	PBE
Martinez-Ruiz [48]	4.3	108	0.5	PBE
Bohnen [42]	4.30	112	–	PBE
Soon [64]	4.34	104	–	PBE
Soon [49]	4.32	104	0.64	PBE
Ruiz [50]	4.43	100	9.7	HF
Ruiz [50]	4.28	93	–	HF+LYP
Heinemann [60]	4.27	–	2.02	HSE06
Scanlon [65]	–	–	2.12	HSE
Tran [61]	4.27[a]	–	0.79–2.77	PBE0
Bruneval [66]	–	–	1.34	G_0W_0
Bruneval [66]	–	–	1.97	scGW
Filippetti [53]	4.23	–	1.8	SIC
Kotani [67]	–	–	1.97	scGW
Lany [68]	–	–	2.03	GW+V_d
Experiment [10]	4.27	109–114	2.17	–

[a]These calculations were performed at the experimental value of the lattice constant.

A wider range of low-index surfaces has been probed using DFT methods than experimentally [77]. These theoretical works predict that the lowest energy structure in conditions of high O_2 pressure is $Cu_2O(111)$ with the unsaturated Cu_{cus} atom removed. At low O_2 pressure, instead, the $Cu_2O(110)$ surface with a CuO-like surface reconstruction is the most stable (Fig. 2c). While the $Cu_2O(111)$ structure has already been observed experimentally [54], the (110) surface has yet to be studied. It is thus evident that there is scope for further experimental work on this topic, to confirm the computational predictions or to propose new reconstructions. Surface-sensitive techniques such as STM and LEED would be best suited to this aim. Moreover, theoretical methods would be well suited to understand the reason behind the transitions between different reconstructions at different conditions of temperature and pressure.

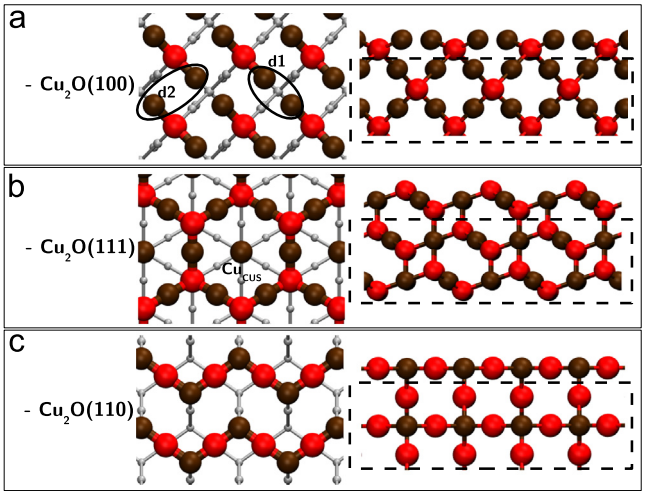

Fig. 2. Structure of the Cu-terminated $Cu_2O(100)$, O-terminated $Cu_2O(111)$ and CuO-terminated $Cu_2O(110)$ surfaces. O atoms are shown in red and Cu atoms in brown. Atoms below the surface layer are depicted in grey in the top views (on the left-hand-side) and enclosed in a box in the side views (on the right-hand-side). (a) Top and side view of a copper terminated $Cu_2O(100)$ slab, consisting of alternating layers of O and Cu atoms. The surface copper atoms 'sink' towards the O-atoms plane and form Cu–Cu dimers (indicated by d1). The second dimer formed in order to obtain the $(3\sqrt{2}\times\sqrt{2})R45^\circ$ reconstruction is labelled d2. (b) Top and side view of the O-terminated $Cu_2O(111)$ surface. The surface layer presents an hexagonal structure with an unsaturated copper atom Cu_{cus} in the middle of each hexagon. (c) Top and side views of the CuO terminated $Cu_2O(110)$ surface. (For interpretation of the references to colour in this figure caption, the reader is referred to the web version of this paper.)

3.3. CuO bulk properties

In CuO, the copper atom has oxidation state Cu^{2+}. The unit cell has monoclinic symmetry [81] (see Fig. 1) and it contains four CuO dimers in the crystallographic unit cell, and two CuO units in the primitive cell. Each copper atom is located in the centre of an oxygen parallelogram. Each oxygen atom, in turn, has a distorted tetrahedral copper coordination. CuO is a p-type semiconductor [82–85] and it is antiferromagnetic in its ground state [86–89].

From a DFT point of view, standard XC functionals alone are not accurate enough to reproduce the distorted nature of the lattice, and, upon structural relaxation, they produce an orthorhombic rather than a monoclinic structure [90]. However, the use of more sophisticated functionals [91,60,92,90,93,52] allows for the reproduction of the triclinic structure and good agreement with experiments on structural and vibrational data [94–97] (see Table 2).

The research focus for CuO has been for a long time on its optical properties, for photothermal and photoconductive applications, and on magnetic and phase stability properties, for possible high-temperature superconducting applications. The electronic properties of CuO, instead, have been studied only more recently. The band gap of CuO has been experimentally measured

Table 2
Calculations of the CuO bulk structure (lattice parameters a, b, c in Å, angle β (between the a and c axes) in degrees, magnetic moment m_B in Bohr magnetons and band gap in eV. The S in the functional name indicates spin-polarised calculations. All calculations featuring the Hubbard U ($+U$ in the functional name) have been done with the so-called 'Dudarev approach' [107], which requires one parameter, $U-J$ (in eV).

Ref.	Lattice (a, b, c) (Å)	β (°)	m_B (μ_B)	Band gap (eV)	XC
Peng [90]	4.05, 4.06, 5.06	90.02	0.0	0.0	LSDA
Peng [90]	4.56, 3.27, 4.96	100.2	0.63	1.32	LSDA+U ($U-J$=7.5)
Anisimov [98]	–	–	0.66	1.9	LSDA+U ($U-J$=6.52)
Debbichi [91]	4.55, 3.30, 4.90	99.65	–	–	LSDA+U ($U-J$=6.52)
Ekuma [99]	4.68, 3.42, 5.13	90	0.68	1.25	DFT+U ($U-J$=7.14)
Heinemann [60]	4.59, 3.35, 5.03	99.39	0.66	1.39	LDA+U ($U-J$=6.52)
Wu [93]	4.55, 3.34, 4.99	99.51	0.6	1.0	LSDA+U ($U-J$=6.52)
Hu [92]	–	–	0.63	1.1	GGA+S+U ($U-J$=6.52)
Jiang [100]	4.68, 3.42, 5.13	99.54	0.80	–	GGA+U ($U-J$=4.5)
Nolan [101]	4.39, 3.85, 5.18	–	0.53–0.7	0.17–2.11	GGA+S+U ($U-J$=3-9)
Svane [102]	–	–	0.65	1.43	SIC-LSDA
Szotek [103]	–	–	0.64	1.0	SIC-LSDA
Filippetti [104]	6.35, 3.42, 7.49	99.54	0.72	2.2	pseudo-SIC
Heinemann [60]	4.513, 3.61, 5.14	97.06	0.54	2.74	HSE06
Rödl [105][a]	–	–	0.55–0.70	1.1–3.9	PBE+U+G_nW_n ($U-J$=4)
Rödl [105][a]	–	–	0.66–0.70	3.1–4.1	HSE06+G_nW_n
Lany [68]	–	–	–	1.19	GW+V_d
Exp.	4.68, 3.42, 5.13 [81]	99.54 [81]	0.68	1.2–1.9 [10,41,84,106,85]	–

[a]Experimental lattice parameters are used. The range in the reported results is due to the different flavours of the GW approximation used.

to be 1.2–1.9 eV [10,41,84,106,85], with the results depending on the sample preparation and on the measurement techniques used. Computationally, the band gap is well reproduced with the LDA+U approach (see Table 2), however the results depend strongly on the value of U while the HSE06 hybrid functional overestimates the gap by approximately 1 eV [60].

3.4. CuO surfaces

The potential use of CuO nanostructures for catalysis, sensing, superhydrophobicity and many other applications [108] requires a good knowledge of the surfaces involved in these processes. Only one experimental study has been performed to date on CuO surfaces. In this work, it was found, using LEED, that the CuO(100) surface in UHV conditions does not present a reconstruction [109].

DFT studies (using a GGA functional with the Hubbard U correction combined, in some cases, with *ab initio* thermodynamics) of the stoichiometric and of some defective surfaces have been performed [92,110,111]. CuO(111) is the most stable surface also compared to defective CuO structures with surface and subsurface vacancies [110]. It has a surface energy $\gamma = 0.74\ J/m^2$, which is much higher than the lowest energy Cu_2O surface [77]. CuO(111) is the most stable surface for all oxygen partial pressures, except for a narrow range at very low O_2 pressures, where the Cu-terminated CuO(110) surface is favourable. The energy order of the stoichiometric surfaces is $(111) < (\bar{1}11) < (011) < (101) < (110) < (010) < (100)$ (shown in Fig. 3) [92]. The highest surface energies (2.28 J/m^2 for CuO(100)) are seen for systems, such as (010) and (100), with the largest separation between anionic (O) and cationic (Cu) layers which give rise to large interlayer electrostatic fields. Among the non-stoichiometric surfaces, the O- and Cu-terminated CuO(110) and CuO(100) are more stable than their stoichiometric counterpart for high (O-terminated) and low (Cu-terminated) oxygen pressures [92].

While important information on stoichiometric and defective CuO surfaces has been obtained using computational methods, experimental data are lacking and there is room for work to be performed in order to either confirm these predictions or to suggest more possible structures.

4. Initial stages of oxidation: oxygen adsorption on clean copper surfaces

The growth of an oxide can occur when a metal surface comes into contact with an oxygen-rich environment. The reaction sequence leading to oxidation of a clean metal surface is generally accepted to be oxygen chemisorption, nucleation and growth of the surface oxide, and bulk oxide growth.

Oxygen adsorbs dissociatively at room temperature on Cu (100), (110) and (111) [114], with barriers of $\sim$0.1 eV for (100) [115], 0.1–0.3 eV for (110) [116–119] and 0.1–0.2 eV for (111) [120–122]. However, even on the very reactive Cu (100) and (110) oxygen binds molecularly at low temperature [123,124], below 50 K and 100 K, respectively. On Cu(111) dissociation is not seen to occur below 170 K [125].

It is well known that clean copper surfaces in vacuum do not reconstruct [126]. However, exposure to oxygen pressure which is low enough not to trigger the formation of oxide-like structures induces reconstructions. We will discuss the details of these reconstructions below, and whether they are important to the initial stages of oxidation is still openly debated. It has been speculated that a reconstructed, O-saturated layer must form before the onset of oxidation, since dwell times, i.e. the lapse of time between the beginning of

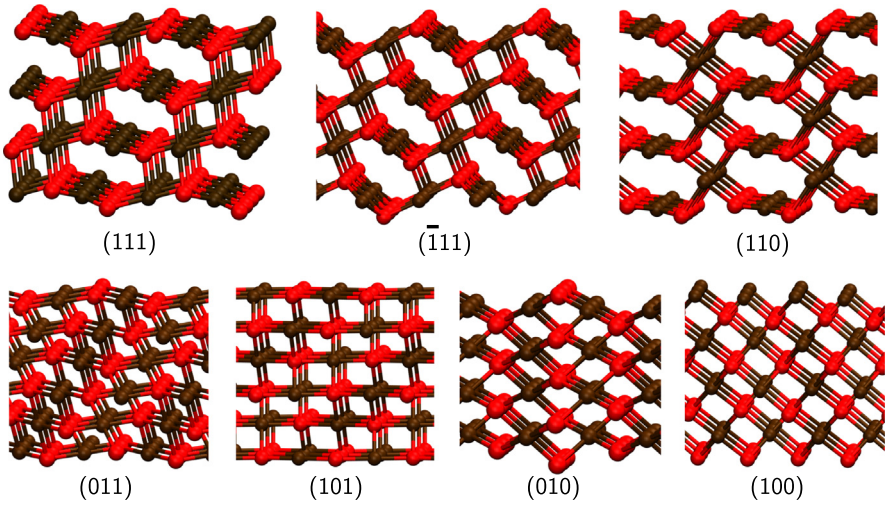

Fig. 3. Side views of CuO slabs showing the structure of stoichiometric cupric oxide CuO surfaces. They are shown in order of increasing surface energy (left to right, top to bottom), as calculated using *ab initio* calculations, using the GGA + U method [92]. Copper is shown in brown, oxygen in red. (For interpretation of the references to colour in this figure caption, the reader is referred to the web version of this paper.)

oxygen deposition and observation of oxide formation, of up to 30 min have been observed [127–129]. Moreover, evidence of the existence of the reconstructed copper surfaces and of subsurface growth of the oxide before the onset of island formation has been produced using STM on Cu(100) [130] and Cu(111) [131]. DFT calculations have shown that, on Cu(100), subsurface oxide-like structures are more easily produced when the surface already has pre-adsorbed oxygen atoms, thus suggesting that the reconstruction facilitates oxide formation [132]. However, it has also been shown that upon exposure to oxygen at higher pressures [133] copper oxide formation at step sites occurs without prior surface reconstruction thus opening the debate about whether direct formation of oxide islands can occur without the formation of an O/Cu overlayer.

In the following section, the very initial stage of the oxidation process, i.e. the chemisorption of oxygen onto copper surfaces is reviewed. A summary of the overlayer structures formed on Cu after O-dosing is shown in Fig. 4. Cu(100) presents two main reconstructions, one with $c(2 \times 2)$ symmetry (Fig. 4b) and a missing-row reconstruction (Fig. 4c), which are discussed in depth in Section 4.1. The overlayer structures for Cu(110) are the $c(6 \times 2)$ phase (Fig. 4e) and the added-row reconstruction (Fig. 4f), discussed in Section 4.2. The O/Cu(111) system, presented in Section 4.3, shows a distorted hexagonal structure resembling the $Cu_2O(111)$ surface (Fig. 4h).

Oxygen adsorption on clean copper has been extensively studied experimentally and computationally, and it has been the subject of a number of reviews over the years, *e.g.* see Refs. [134,114]. Here we focus only on the studies which are relevant in order to understand the onset of copper oxidation on the Cu(100), (110) and (111) surfaces and on the most recent developments in the field.

4.1. Cu(100)

Oxygen adsorption on Cu(100) has been widely studied [114,130,135], and an interesting variety of structures is formed depending on temperature and coverage, as shown in the phase diagram in Fig. 5a.

At low temperatures (up to 100 K) and low coverage (~ 0.1 monolayers, ML, defined as one adsorbed oxygen atom for every surface copper atom) experimental and computational evidence has shown that incident oxygen molecules dissociate with the oxygen atoms adsorbing at the hollow site [136–141]. These dissociated oxygen atoms stabilise chemisorption of further incoming oxygen molecules at higher coverages [142,143,124,144].

Below 473 K, two overlayer structures form: a $c(2 \times 2)$ phase [130,145–148] at a coverage of ~ 0.3 ML and a $(2\sqrt{2} \times \sqrt{2})R45^\circ$ missing-row (MR) reconstruction [149–158] at ~ 0.5 ML. In the $c(2 \times 2)$ phase (shown in Fig. 4b) the oxygen atoms occupy four-fold hollow sites on Cu(100) and form nanometre-sized $c(2 \times 2)$ domains separated by oxygen-deficient zig-zag shaped boundaries. The MR reconstruction (Fig. 4c, 5b) can be viewed as a $c(2 \times 2)$ structure with each fourth [100] row of Cu atoms missing. Between 0.3 and 0.5 ML, Cu atoms are ejected from the $c(2 \times 2)$ domains [159,132] and MR islands start forming on terraces, until, at 0.5 ML coverage, a network of missing-row reconstruction islands covers the whole surface [130,145].

At high temperatures ($473 < T < 1000$ K) a 'disordered' $c(2 \times 2)$-like state, with 25% of randomly distributed vacancies in the top Cu layer, forms at 0.5 ML coverage, instead of the MR reconstruction [160]. No further oxygen adsorption occurs above 0.5 ML for experiments at very low pressures ($< 10^{-7}$ Torr). However, at higher pressures, further exposure of the surface to O_2 leads to growth of oxide in the subsurface regions, while the surface still exhibits the MR reconstruction [130,153], validating the hypothesis that oxygen-induced surface reconstruction is indeed the first step of oxide growth. DFT studies combined with *ab initio* thermodynamics [139,161] confirmed that the $c(2 \times 2)$ and MR reconstructions are indeed the most stable structures prior to the onset of bulk oxidation.

The transition between the two low-temperature reconstructions is still not fully understood and it has been tentatively explained in terms of stress relief, electronic structure and

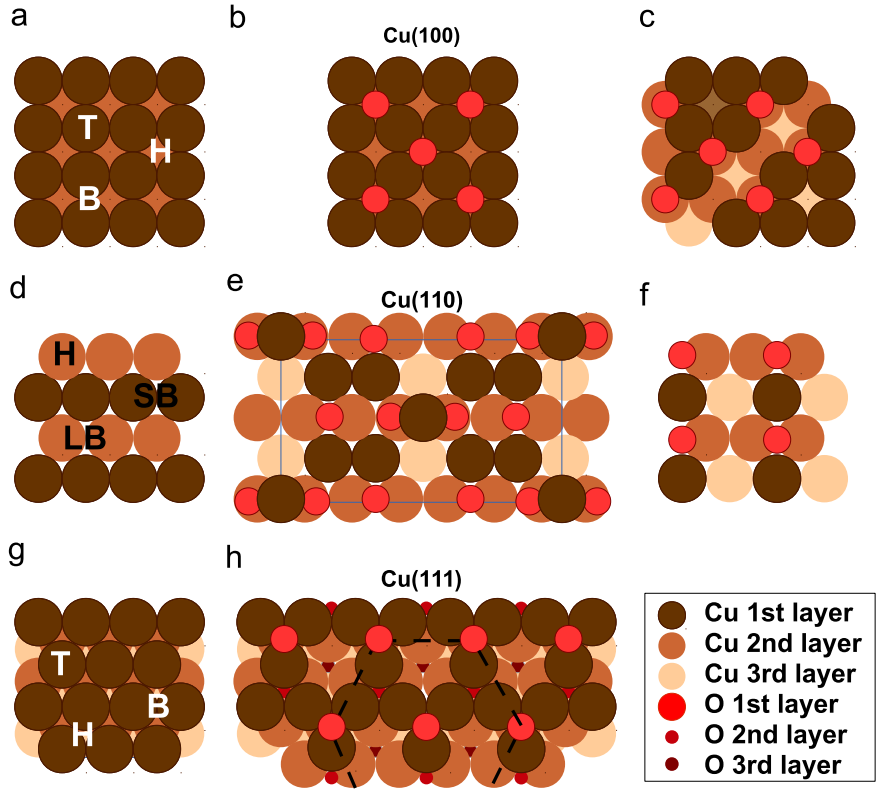

Fig. 4. Overview of the structures formed by oxygen on different copper surfaces, at low oxygen exposures. (a, d, g) Clean surfaces of Cu(100), Cu(110) and Cu (111). T, H, B, SB and LB indicate respectively the top, hollow, bridge, short bridge and long bridge sites for adsorption. (b) $c(2 \times 2)$ overlayer structure seen on Cu (100) at coverages < 0.3 ML. (c) $(2\sqrt{2} \times \sqrt{2})R45^{\circ}$ missing-row reconstruction seen on Cu(100) at coverages > 0.5 ML. (e) $c(6 \times 2)$ structure observed on Cu (110) at low coverage and high temperature or at high (2/3 ML) coverage. The blue box indicates the unit cell, for clarity. (f) (2×1) added-row reconstruction observed on the Cu(110) surface. (h) $Cu_2O(111)$-like reconstruction of the Cu(111) surface having hexagonal geometry as shown by the dashed line. Two layers of subsurface oxygens are shown. Distorted variations of this reconstruction have been observed experimentally [112,113]. (For interpretation of the references to colour in this figure caption, the reader is referred to the web version of this paper.)

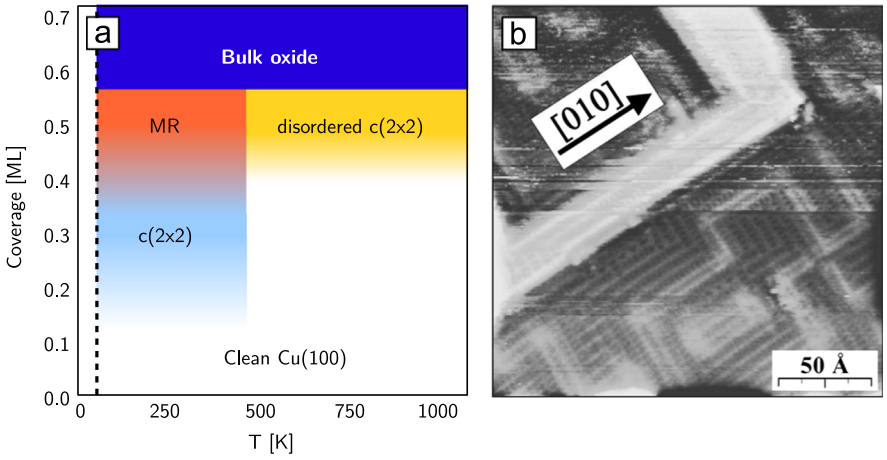

Fig. 5. (a) Summary of the structures formed on Cu(100) after oxygen exposure. The dashed line indicates the lowest temperature at which experiments have been performed (30 K) for this system. The areas in white represent domains where no ordered oxygen overlayers form. For low temperatures, at coverages of ~ 0.3 ML the $c(2 \times 2)$ structure forms and at ~ 0.5 ML the missing row (MR) reconstruction is seen. At intermediate coverages both structures exist. At high temperatures a 'disordered' $c(2 \times 2)$ structure occurs. At coverages over 0.5 ML subsurface oxide starts to grow. (b) STM image of Cu(100) after O_2 exposure ($P = 3.7 \times 10^{-2}$ mbar, T=373 K). A $(2\sqrt{2} \times \sqrt{2})R45^{\circ}$ island and a zigzag phase boundary (bright stripe) are visible. The missing rows of Cu run along the $\langle 001 \rangle$ directions and are imaged as depressions. Taken from Ref. [130].

electrostatics. Experimental and DFT studies [162,163] have shown that compressive surface stress increases with oxygen adsorption and that, for the same coverage, it is much larger in the $c(2 \times 2)$ than in the MR reconstruction. Therefore, transition to the MR phase at high oxygen coverage (and therefore high stress) conditions provides surface stress relief. From an

electronic structure point of view, O(p)–Cu(d) orbital hybridisation of neighbouring O and Cu atoms [164,165] stabilises the MR over the $c(2 \times 2)$ phase. Alternatively, the effective charge on the O atoms has been pinpointed as the source of the instability of the low-coverage phase by Colbourn et al., who found O to be negatively charged by 0.9 e^-. However, more recent calculations have found the negative charge on O to be 0.3 e^- for both structures, too small to drive any surface instability [165]. Finally, long-range Coulomb interactions play a critical role in determining the geometry of the Cu (100) overlayers [166–170]. Indeed, repulsion between O adatoms and Cu and O adatoms is the cause of the small size of the $c(2 \times 2)$ domains at low coverages. At higher coverages, where the repulsion cannot drive the O adatom away from other O or Cu atoms, the MR phase transition occurs to minimise high O–O repulsion. Further work is needed on all of these points in order to clarify the phase transition mechanism.

The transition between the ordered MR to the high-temperature 'disordered' $c(2 \times 2)$ reconstruction has been explained by means of DFT as the result of the diffusion of Cu surface vacancies from an ordered array in the MR system to random positions as the temperature increases [160].

An intermediate added row structure was predicted by Kangas et al. [171] which has energies comparable to the MR reconstruction. This reconstruction has however not yet been observed experimentally, possibly because the right conditions of temperature and pressure have not been used [130]. *Ab initio* thermodynamics calculations could approximately establish at which experimental conditions this reconstruction is expected and could thus inform further experimental work.

It is important to note that simulations have shown that the MR structure is a necessary step towards the formation of a Cu_2O-like structure [132,172]. Indeed, Cu_2O-like structures were found to form on the MR reconstruction upon O adsorption which were not found on the non-reconstructed surface, thus confirming the experimental results of Lahtonen et al. [130] and fitting well with the work of Zhou et al. [173], who finds the presence of a two-layer thick oxide before the formation of oxide islands of the Cu(100) surface (see Section 5.1).

In summary, three reconstructions can form on Cu(100) upon oxygen adsorption, as shown in Fig. 5. Of these, the MR reconstruction is the most stable at room temperature, for coverages $\sim$0.5 ML. Experimental and computational evidence has shown that the formation of this reconstruction is the first step towards the formation of the bulk oxide.

4.2. Cu(110)

Molecular oxygen dissociates when deposited on Cu(110) at temperatures above 45 K [174]. Upon dissociation of the O_2 molecules a number of overlayer structures are observed, including an added-row (2×1) structure (Fig. 4f) which is formed at an oxygen coverage of 0.5 ML [114,157,175–177]. Another structure, $c(6 \times 2)$ (Fig. 4e), has been reported at high coverage ($\sim 2/3$ ML) [178–181,157,182,177,183,184] or at lower coverage but higher temperature [185].

The (2×1) phase forms via the creation of Cu–O–Cu–O chains along the [001] direction of the substrate, which eventually become the 'added rows' on top of the clean substrate at a coverage of 0.5 ML. The chains start forming above 70 K but do not fully organise until $\sim$200 K [174]. They are formed from mobile chemisorbed O atoms and Cu adatoms which leave from step edges and diffuse across the terraces [186,150,187–189,174,190]. The experimental barrier calculated for the formation of these strings, 0.22 ± 0.01 eV [164], is close to the DFT-calculated barriers for Cu (0.25 eV) and O (0.15 eV) diffusion [191].

At oxygen coverages between 0.05 and 0.45 ML these Cu–O–Cu–O chains self-organise in a periodic array (called a supergrating) with a spacing varying between 60 and 140 Å [192–194,150,195]. The dependence of the period of the supergrating as a function of oxygen coverage has been explained in terms of elastic [196–201] and electrostatic [202] interactions. In the first case, the supergrating is assumed to arise from the mismatch between the preferred period of the Cu–O–Cu–O chains and the period of the Cu(110) substrate in the [001] direction. Instead, from an electrostatic point of view, it has been shown that the difference in work function between the clean and reconstructed sections of metal surfaces can stabilise periodic domain structures. It could indeed be possible for both mechanisms to be at play.

The stability of the (2×1) reconstruction at 0.5 ML has been established computationally by means of semi-empirical and DFT calculations, where it has been found to be energetically favourable with respect to the unreconstructed surface [164,203,191,116] and to an alternative added row (4×1) geometry [200]. DFT simulations with *ab initio* thermodynamics [139,204,184] found that the Cu–O added row reconstruction is favoured at low oxygen exposures, whereas at higher oxygen exposures, a transition to the $c(6 \times 2)$ structure is predicted to occur. Thus, experiment and theory are in qualitative agreement, although the absolute transition pressures vary enormously (by 10 orders of magnitude). Since it is a major challenge for current DFT XC functionals to accurately predict adsorption energies and the underlying value of the adsorption energy has a huge impact on subsequent pressure estimates, such a quantitative discrepancy is not uncommon [205–207]. The barrier to transition between the two structures has been calculated to be fairly high at 1.41 eV, which seems to explain why this phase is observed only at high temperatures.

A large body of work has focused on understanding the surface electronic states of the added row reconstruction, using both experimental methods such as photoemission spectroscopy [208–211] and theory [211–213]. The character of the O–Cu bonding is found to be predominantly ionic, and the surface O($2p$) orbitals hybridise strongly with the Cu($3d$) states, forming bonding and antibonding linear combinations, with the antibonding bands not having been identified unambiguously yet.

There is no evidence so far on how the observed reconstruction relates to the initial formation of the oxide, if at all. DFT

calculations of subsurface oxygen added beneath both reconstructed surfaces have found that when an O coverage of 1 ML is reached, subsurface oxide formation in the tetrahedral interstitial sites is predicted to occur [214,215]. The presence of oxygen in the tetrahedral site has been linked to oxide formation (since the O in Cu_2O resides in the tetrahedral sites), and therefore this is a possible mechanism for the initial formation of the oxide, which should however be confirmed by experimental or further computational work.

4.3. Cu(111)

The clean (111) surface has the lowest surface energy for copper and it is less reactive compared to the other low-index Cu surfaces. It is therefore less studied for oxygen adsorption [112,113,128,142,143,216–224]. No ordered structures are observed experimentally for low oxygen exposure [218,128,219,225]. Indeed, also DFT studies have found that oxygen adsorbs preferentially at the threefold hollow site for coverages up to 0.75 ML, without forming periodic overlayer structures [120,49,226,227].

At higher coverage, the adsorbed oxygen and copper adatoms that are ejected from step edges and terraces [223,224,131] start forming overlayer structures, before the onset of epitaxial growth (see Section 5.3). Two main classes of reconstructions have been proposed for O/Cu(111). The first, seen in LEED studies, involves a Cu(100)-like overlayer, incommensurate with the underlying unreconstructed Cu(111) surface, with the oxygen atoms occupying the hollow sites [228–230]. This structure is however metastable and changes to the most thermally stable '29' phase presented below [231].

The second class comprises two long-range ordered structures [221,112], the so-called '29' and '44' superstructures. They have, respectively, $(\sqrt{13}R(46.1^\circ \times 7R21.8^\circ)$ and $(\sqrt{73}R5.8^\circ \times \sqrt{21}R-10.9^\circ)$ symmetry and very large surface unit cells, 29 and 44 times larger than the (1×1) cell of clean Cu (111). They exhibit an honeycomb pattern formed by distorted hexagonal units of the 'ideal' $Cu_2O(111)$ overlayer shown in Fig. 4h. The oxide-like overlayer structure has been confirmed by STM [223], X-ray absorption studies [113], DFT and *ab initio* molecular dynamics [78,49]. This differs from the behaviour of other O/transition metal systems such as O/Ag(111) [232–235] and O/Pd(111) [236], where chemisorbed oxygen adlayers form, before the formation of a surface oxide. Other systems, such as O/Ru(0001) [237] and O/Rh(111) [238,239], instead never form a surface oxide layer before the onset of bulk oxidation.

Therefore, both experimental and computational studies point to the formation of hexagonal or quasi-hexagonal structures on the Cu(111) surface upon oxygen adsorption, structures which can be viewed as the initial layer of a Cu_2O (111) film and which can potentially act as a template for the growth of further $Cu_2O(111)$ layers.

5. Oxide film growth

When copper surfaces are exposed to a continuous flow of oxygen for a long time oxidation is expected to occur. It is known in general, from well-defined surface science studies of metals, such as those discussed in Section 4, that the O/metal structure which forms at the onset of oxidation can be distinct from the bulk oxide surface structure [15,234,240].

In order to understand the microscopic details of the onset of oxidation, experiments have been performed in controlled laboratory conditions, where the orientation of the surface, temperature and oxygen pressures can be tuned to the required values. The formation of the oxide has been directly observed with TEM, and its structure analysed with LEED and ellipsometry. At the oxygen pressure, temperature and exposure times used in these studies, only cuprous oxide is expected to form [39,241,242]. We review studies showing that the growth of cuprous oxide on low-index copper surfaces is epitaxial with the substrate [243,244,15,245,246], through nucleation and coalescence of nano-islands [247,248,216,128,243,127,217] (as schematically represented in Fig. 6). However, the mechanism of formation of the islands and the resulting shapes and growth rates are strongly dependent on the Cu substrate, as shown in Section 5.1 for Cu(100), Section 5.2 for Cu(110) and Section 5.3 for Cu(111). Key experimental findings are summarised in Tables 3–5. Next, the existence of preferential oxidation sites is discussed in Section 5.4. The kinetic models for the nucleation and coalescence of the nano-islands and for the growth of the oxide thin film are reviewed in Sections 5.5 and 5.6.

Growth of the oxide in ambient conditions, when the copper surface is exposed to humid air, has also been extensively studied. The body of work addressing this issue is reviewed in Section 5.6 and summarised in Table 7.

Finally, studies on the initial growth of CuO are reviewed (Section 5.8).

5.1. Oxide nano-islands: Cu(100)

As for the formation of O/Cu overlayers, Cu(100) is the most extensively studied surface, both experimentally and computationally. Copper oxidation on this surface proceeds, for low oxygen partial pressures ($P \sim 10^{-4}$ Torr), through the formation of epitaxial oxide islands, i.e. $Cu_2O(100) \parallel Cu(100)$ [249,250,129,14,247,127,251] whereas, for high oxygen pressures (above 150 Torr), island nucleation is not epitaxial [252]. These islands have a (6×7) lattice misfit configuration [253,241] and they grow and coalesce with further oxygen deposition. The shape of the islands depends on temperature [254] in a rather interesting manner as shown in Fig. 7. Below 350 °C only triangular islands are observed, whereas between 400 and 550 °C the shape changes to round or square. At around 600 °C the islands start to grow until, at a critical size of $\sim$110 nm, when they switch to a quasi-one-dimensional elongated rod shape. Between 650 and 800 °C pyramid-shaped islands are observed and between 800 and 1000 °C hollow pyramids form [255]. The big effect of temperature on the morphology of the islands could be either due to the dependence of copper and oxygen diffusion on temperature or to changes in interfacial strains and in the mechanical properties. Indeed, the transition between the round/square to

rod shape (Fig. 7b,c) and pyramid to hollow rod/pyramid shape (Fig. 7d,e) has been explained as a competition between the surface energy and the strain of the islands due to the mismatch between the clean metal and the oxide lattices [256], following the so-called Tersoff-Tromp [257] energy model.

TEM, XPS and AES studies looking at the cross section of an oxidising Cu(100) single crystal under low oxygen partial pressure [173,258,129,259] have revealed that the oxide islands form on top of an oxide wetting layer. The wetting layer itself has a $(\sqrt{2} \times 2\sqrt{2})R45^\circ$ missing row reconstruction and forms from the Cu atoms ejected by the missing row reconstruction of the substrate (described in Section 4.1) and the further oxygen deposited on the substrate [258]. Island growth also occurs beneath the surface, in good agreement with the already reviewed results by Lahtonen et al. [130] (Section 4.1) who observed subsurface oxide growth for oxygen coverages above 0.5 ML and pressures above $\sim 10^{-7}$ Torr.

In general, when a metal is capable of forming uniform subsurface oxides (as in the case of Ag(110) [260] and Ru (0001) [261]), oxide growth proceeds uniformly, rather than via island formation. The reason for the island formation on top of the wetting layer is found in stress mismatch between the Cu(100) substrate and the Cu_2O(100) film [173].

The transition between the O/Cu(100) system described in Section 4.1 and the oxide islands has been studied to some extent with DFT, and although the full transition has not been modelled yet, insight has been gained into the mechanisms at play. On the MR reconstructed surface, sub-surface adsorption becomes favourable for O coverage above 1.0 ML, with low barriers for the transport of oxygen atoms below the surface [262–264]. Sub-surface oxygen atoms below the missing-row reconstruction adsorb in the tetrahedral interstitial sites, and thus form an oxide-like structure, unlike the case of sub-surface oxygen atoms below non-reconstructed surfaces, which adsorbs in the octahedral site [172]. However, the limiting factor for the oxidation of Cu(100) is the dissociation and on-surface diffusion of the oxygen molecule. The dissociation of the oxygen molecule, although involving a low barrier on the clean Cu(100) [137], is blocked by the on-surface oxygen on the reconstructed surface [265]. Therefore, O_2 dissociation on the reconstructed surface requires the diffusion of the oxygen molecule towards either a high-Cu concentration area [167] or vacancies and surface defects [266,267] where the dissociation barrier is lower. Diffusion of O and Cu atoms on the MR reconstructed surface is slow, having barriers of 1.4 eV for oxygen and 2.0 eV for Cu [167]. The high barriers and slow diffusion make these processes difficult to simulate. Indeed, Devine et al. [268] successfully simulated oxygen molecule dissociation on the clean Cu(100) surface with bond-order potentials, however they did not see any dissociation event on the missing-row reconstructed surface within their (short) 10 ps of molecular dynamics. This highlights the difficulty of reproducing these complex phenomena which include diffusion of oxygen molecules, dissociation, diffusion of oxygen and copper atoms on and through the surface using standard computational approaches. To this end, the combination of an accurate reactive potential with methods which allow for rare events to be probed, such as metadynamics [269] are possibly a way to go for this type of system.

5.2. Oxide nano-islands: Cu(110)

The islands formed on Cu(110) single crystals after being exposed to low pressure oxygen ($P \sim 10^{-4}$ Torr) are also found to be epitaxial with the substrate [193], up to an oxygen partial pressure of 50 Torr [252]. Also on Cu(100) a $\sim$4 Å wetting layer, occurring before island nucleation, is observed [274]. The island morphology and the time required to reach saturation density depend on temperature, with higher temperatures requiring much shorter time to saturation. Between 450 and 650 °C the lateral size of the islands is almost constant (200–250 nm), however the islands were found to thicken considerably (24–40 nm) beneath the Cu surface, showing that the rise in temperature greatly enhances

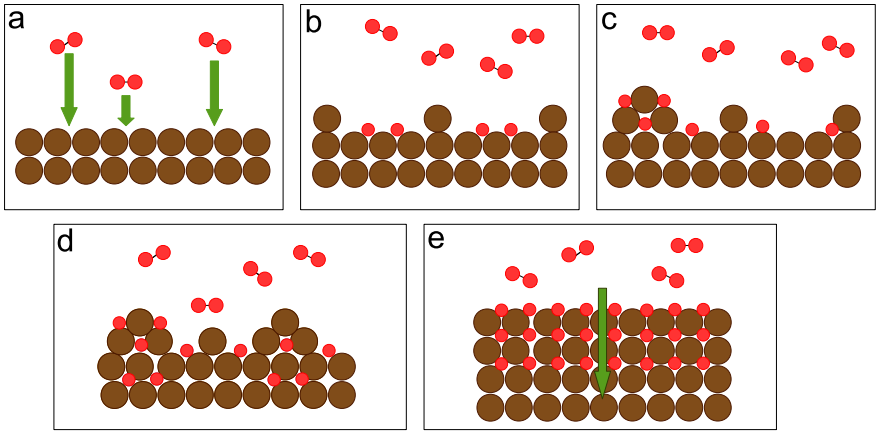

Fig. 6. Schematic illustration of the stages of growth of a copper oxide film on copper. (a) Gas-phase oxygen molecules and clean copper surface. (b) Upon oxygen adsorption the copper surface reconstructs. (c) Nucleation of oxide islands upon diffusion of oxygen on the reconstructed surface, until the island saturation density (N_{sat}) is reached. (d) Growth of the oxide islands. As the islands grow bigger direct oxygen impingement on the islands starts playing a more important role. (e) After the islands coalesce oxide growth proceeds through interfacial diffusion of oxygen.

Table 3
Experimental results of copper oxide formation in ultra-high vacuum on Cu(100). Experimental conditions and techniques have been listed, together with a summary of the main result of each study. d is the sample thickness (a – sign indicates it was not reported in the paper).

Reference	d (nm)	Surface preparation	Exp. conditions	Technique	Result
Brockway [247] (1972)	90	Annealing in H_2 at $T=$ 630 °C	$P=10^{-3}>$ Torr, $T=525$ °C	TEM	Epitaxial growth of oxide islands
Heinemann [127] (1975)	80	Annealing, argon ion sputter etching	$P=5\times10^{-3}$ Torr, $T=425$ °C	TEM	Epitaxial growth of square and hexagonal oxide islands
Stefanov [251] (1988)	–	Ion bombardment and heating under UHV	$P=10$ to 2×10^{6} L, $T=-130$–180 °C	HREELS, XPS	Cu_2O formation at oxygen exposures between $10^{5}-2\times10^{6}$ L
Yang [249] (1997)	40	Annealing in methanol vapour at $T=350$ °C	$P=1.5\times10^{-5}$ Torr	TEM	Rate of growth of the oxide islands $\propto t^{1.3}$
Yang [129] (1998)	100	Annealing in UHV/CH_4O vapour at $T=350$ °C	$P=1\times10^{-5}-1\times10^{-4}$ Torr	TEM	O monolayer forms before growth of the oxide islands
Yang [270] (1998)	60	Annealing in methanol vapour at $T=350$ °C, $P=5\times10^{-5}$ Torr	$P=5\times10^{-5}$–760 Torr, $T=60$–600 °C	TEM	Epitaxial island formation after surface reconstruction
Yang [250] (1998)	100	Annealing in CH_4O vapour at $T=350$ °C, $P=5\times10^{-5}$ Torr	$P=5\times10^{-4}$ Torr, $T=290$–435 °C	TEM	Nucleation of islands promoted by O diffusion
Yang [271] (1999)	100	Annealing in CH_4O vapour at $T=350$ °C, $P=5\times10^{-5}$ Torr	$P=1\times5^{-5}$–5×10^{-4} Torr, $T=70$–600 °C	TEM	Preferential nucleation site at the edge of pits
Yang [259] (2001)	60–100	Annealing in CH_4O vapour at $T=350$ °C, $P=5\times10^{-5}$ Torr	O_2/H_2O vapour at $P=5\times10^{-4}$ Torr, $T=350$ °C	TEM	Initial surface reconstruction prior to island growth
Yang [14] (2002)	60	Annealing in CH_4O vapour at $T=350$ °C, $P+5\times10^{-5}$ Torr	$P=5\times10^{-5}$–760 Torr, $T=60$–600 °C	TEM	Good agreement of kinetic data with the JMAK model
Zhou [254] (2003)	70	Annealing in CH_4O vapour at $T=350$ °C, $P=5\times10^{-5}$	$P=5\times10^{-4}$ Torr, $T=150$–1000 °C	TEM	Temperature-dependent shape of oxide nano-islands
Eastman [241] (2005)	110–200	Annealing in Ar-2%H_2 at $T=850$ °C, $P=5\times10^{-5}$ Torr	$P=5\times10^{-4}$ Torr, $T=350$–780 °C	X-ray scattering	Epitaxial nano-island formation
Zhou [272] (2005)	70–80	Annealing in CH_4O vapour at $T=350$ °C/vacuum $T=800$ °C	$P=5\times10^{-4}$ Torr, $T=350$ °C	TEM	Island nucleation rate faster on (111) than (110) or (100)
Zhou [273] (2005)	70–80	Annealing in vacuum at $T=550$ °C	$P=5\times10^{-5}$ Torr, $T=350$–900 °C	TEM	Temperature-dependent shape and oxidation rate of the oxide islands
Zhou [255] (2005)	70–80	Annealing in CH_4O vapour at $T=350$ °C/vacuum $T=800$ °C	$P=5\times10^{-4}$ Torr, $T=350$ °C	TEM	Island nucleation rate faster on (111) than (110) or (100)
Lampimaki [258]	–	Ar^+ bombardment, annealing at $T=700$ °C	$P=2.8\times10^{-2}$–160 Torr, $T=30$–100 °C	XPS, XAS, STM	Island formation on top of the missing-row reconstruction for O/Cu(100)
Lahtonen [130] (2008)	5×10^{5}	Ar^+ bombardment, annealing at $T=430$ °C	$P=6\times10^{-7}$ Torr and $T=2.8\times10^{-2}$ Torr, $T=100$ °C	STM	Surface reconstruction and oxide island formation at high O_2 exposure
Zhou [253] (2009)	70	Annealing in Ar/H_2 at $T=700$ °C	$P=5\times10^{-5}$ Torr, $T=700$ °C	TEM	Cu_2O islands, 200/500 nm side. Epitaxial growth with inclined Cu_2O/Cu edges
Zhou [256] (2009)	60	Annealing in vacuum at $T=750$ °C/in CH_4O vapour at $T=350$ °C, $P=5\times10^{-5}$ Torr	$P=5\times10^{-4}$ Torr, $T=600$ °C	TEM	Pyramid to hollow pyramid transition
Zhou [133] (2012)	50	Annealing in H_2 at $T=600$ °C	$P=5\times10^{-5}$ Torr, $T=350$ °C	TEM	Step-edge induced oxide growth.
Luo [252] (2012)	70	Annealing in vacuum at $T=750$ °C/ Annealing in H_2 at $T=350$ °C and $P\sim\times10^{-5}$ Torr	$P=5\times10^{-5}$–760 Torr, $T=350$ °C	TEM	Temperature-dependence on orientation of Cu_2 oxide islands
Zhou [173] (2013)	50	Annealing in H_2 at $T=600$ °C	$P=1\times10^{-3}$ Torr, $T=550$ °C	TEM	Cu_2O Islands growth on an oxide wetting layer nucleated on surface steps

the interfacial diffusion of oxygen [275]. At 700 °C, the (110) surface of clean copper roughens with a step height of ~10 nm [276]. Exposure to oxygen of this rough surface shows the formation of a higher density of oxide islands with a fast nucleation rate but slower lateral growth than for smooth surfaces. This comparison between smooth and rough surfaces supports the idea that the kinetics of nucleation and growth of islands is dependent on the surface diffusion of oxygen atoms on the surface (see Section 5.5).

5.3. Oxide nano-islands: Cu(111)

At room temperature the oxidation of Cu(111) also proceeds through the formation of oxide islands [278,131,223] which, up to a pressure of 75 Torr [252], are epitaxial with the substrate. They present a 5×6 lattice misfit [278,131,223] and they coalesce with continuous oxygen exposure. Three processes of oxide formation are observed [131,223] (Fig. 8): growth from step edges, in-

Table 4
Experimental results of copper oxide formation in ultra-high vacuum on Cu(110). Experimental conditions and techniques have been listed, together with a summary of the main result of each study. d is the sample thickness.

Reference	d (nm)	Surface preparation	Exp. conditions	Technique	Result
Zhou [277] (2002)	70	Annealing in CH_4O vapour at $T = 350$ °C, $P = 5 \times 10^{-5}$ Torr	$P = 8-1 \times 10^{-4}$ Torr, $T = 600$ °C	TEM	Rod-shaped 20 nm-thick islands
Zhou [193] (2003)	70	Annealing in CH_4O vapour at $T = 350$ °C	$P = 5 \times 10^{-4}$ Torr, $T = 300$–450 °C	TEM	Faster initial oxidation rate than Cu(100)
Zhou [276] (2004)	70	Annealing in CH_4O vapour at $T = 350$ °C	$P = 5 \times 10^{-4}$ Torr, $T = 350$–750 °C	TEM	Higher density and slower lateral growth rate of islands on rougher Cu(110) surfaces
Zhou [275] (2004)	70	Annealing in CH_4O vapour at $T = 350$ °C	$P = 5 \times 10^{-4}$ Torr, $T = 750$ °C	TEM	Faster oxidation at higher temperatures
Zhou [272] (2005)	70–80	Annealing in CH_4O vapour at $T = 350$ °C/vacuum $T = 800$ °C	$P = 5 \times 10^{-4}$ Torr, $T = 350$ °C	TEM	Island nucleation rate faster on (111) than (110) or (100)
Zhou [273] (2005)	70–80	Annealing in vacuum at $T = 550$ °C	$P = 5 \times 10^{-5}$ Torr, $T = 350$–900 °C	TEM	Temperature-dependent shape and oxidation rate of the oxide islands
Zhou [255] (2005)	70–80	Annealing in CH_4O vapour at $T = 350$ °C/vacuum $T = 800$ °C	$P = 5 \times 10^{-4}$ Torr, $T = 350$ °C	TEM	Island nucleation rate faster on (111) than (110) or (100)
Luo [252] (2012)	70	Annealing in vacuum at $T = 750$ °C/ Annealing in H_2 at $T = 350$ °C and $P \sim \times 10^{-5}$ Torr	$P = 5 \times 10^{-5}$–760 Torr, $T = 350$ °C	TEM	Temperature-dependence on orientation of Cu_2 oxide islands

Table 5
Experimental results of copper oxide formation in ultra-high vacuum on Cu(111). Experimental conditions and techniques have been listed, together with a summary of the main result of each study. d is the sample thickness (a – sign indicates it was not reported in the paper).

Reference	d (nm)	Surface preparation	Exp. conditions	Technique	Result
Lawless [280] (1956)	–	Electropolishing	$P = 0.8$–760 Torr, $T = 170$–450 °C	XRD	Epitaxial Cu_2O oxide, disordered CuO
Goulden [243] (1976)	2.5–4.0×10^5	Polishing in orthophosphoric acid at 1.4 V	$P = 8 \times 10^{-4}$ Torr, $T = 250$–400 °C	TEM	Epitaxial oxide islands
Ho [217] (1978)	–	Annealing in vacuum at $T = 300$ °C	$P = 10^{-4}$–10^{-7} Torr, $T = 350$ °C	TEM	Epitaxial lamellar growth
Dubois [128] (1982)	–	Annealing in H_2 at $T = 630$ °C	$P = 1 \times 10^{-3}$ Torr, $T = 525$ °C	EM	Epitaxial oxide islands on defect sites
Milne [248] (1984)	50	Polishing, annealing	$P = 10^{-5}$–5×10^{-4} Torr, $T = 300$ °C	RHEED, TEM	Formation of epitaxial oxide islands
Rauh [281] (1993)	50	Deposition by dc heating	$P = 7.5 \times 10^{-4}$–9×10^{-2} Torr, $T = 105$ °C,400 min	Ellipsom	Formation of a Cu_2O film
Matsumoto [223] (2001)	–	Ar^+ sputtering and vacuum annealing at $T = 500$ °C	$P = 10^{-7}$–10^{-5} Torr,RT	STM, LEED	Growth of oxide from step edges
Zhou [272] (2005)	70–80	Annealing in CH_4O vapour at $T = 350$ °C/vacuum $T = 800$ °C	$P = 5 \times 10^{-4}$ Torr, $T = 350$ °C	TEM	Island nucleation rate faster on (111) than (110) or (100)
Zhou [273] (2005)	70–80	Annealing in vacuum at $T = 550$ °C	$P = 5 \times 10^{-5}$ Torr, $T = 350$–900 °C	TEM	Temperature-dependent shape and oxidation rate of the oxide islands
Zhou [255] (2005)	70–80	Annealing in CH_4O vapour at $T = 350$ °C/vacuum $T = 800$ °C	$P = 5 \times 10^{-4}$ Torr, $T = 350$ °C	TEM	Island nucleation rate faster on (111) than (110) or (100)
Zhou [279] (2008)	–	Annealing in vacuum at $T = 800$ °C	$P = 3 \times 10^{-4}$ Torr, $T = 900$ °C	TEM	Growth of oxide hollow pyramidal islands
Zhou [278] (2009)	60	Annealing in CH_4O vapour at $T = 350$ °C/vacuum $T = 800$ °C	$P = 5 \times 10^{-4}$ Torr, $T = 350$ °C	TEM	Epitaxial $C_2O \sim 2.5$ nm-high islands
Leon [131] (2012)	–	Ar^+ sputtering and $T = 550$ °C heating	$P = 10^{-7}$ Torr, RT, pulse injection of air	AES, STM	Oxide growth from step edges
Luo [252] (2012)	70	Annealing in vacuum at $T = 750$ °C/ Annealing in H_2 at $T = 350$ °C and $P \sim \times 10^{-5}$ Torr	$P = 5 \times 10^{-5} - 760$ Torr, $T = 350$ °C	TEM	Temperature-dependence on orientation of Cu_2 oxide islands

terrace growth ($\sim$1.2 Å below the terrace surface) from vacancy islands and growth of on-terrace oxide. The formation of randomly placed islands at low temperature agrees well with the existence of a disordered underlying structure observed for low-coverage oxygen adsorption and analysed in Section 4.3. At higher temperatures [278,223] fast formation of the oxide and fast lateral growth leads to the formation of a two-dimensional oxide structure. This

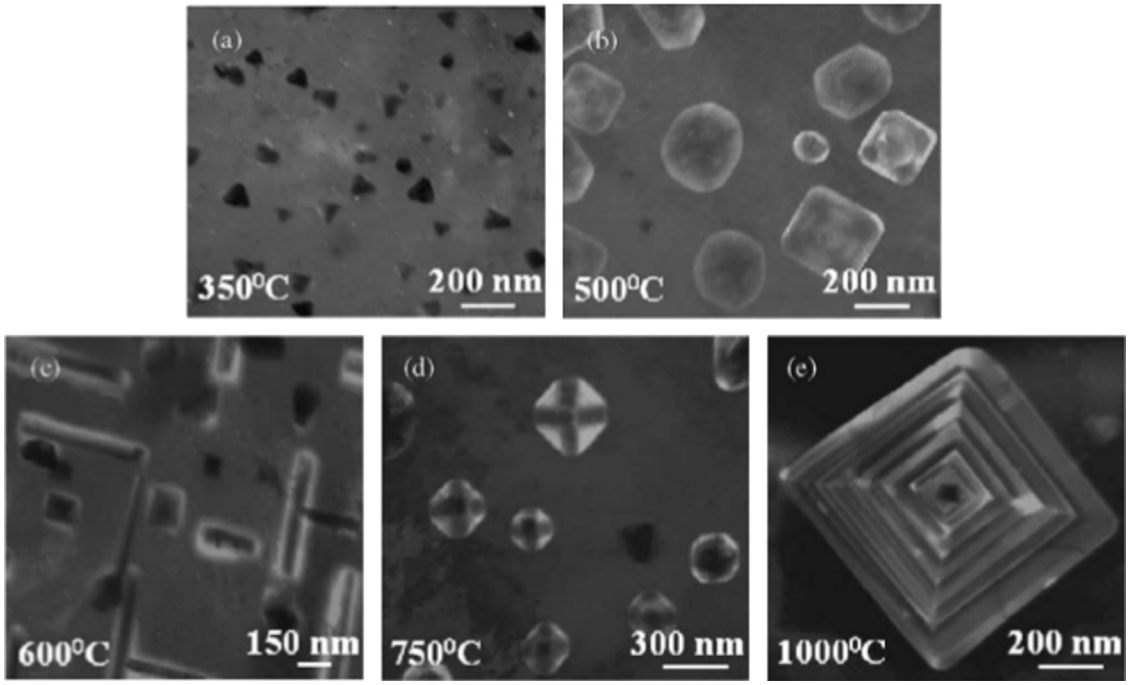

Fig. 7. Oxide islands observed on Cu(100) using *in situ* TEM imaging, for a set of temperatures between 350 and 1000 °C. The oxidation partial pressure is $P = 5 \times 10^{-4}$ Torr. A large variety of island structures are observed, according to the oxidation temperature. Taken from Ref. [254].

uniform growth is templated by the distorted-hexagonal surface reconstruction shown in Section 4.3 [223].

Zhou et al. observed an interesting phenomenon at intermediate temperatures: the islands nucleate close to existing islands, anisotropically elongating along the (110) direction in a percolating manner, as shown in Fig. 9. This 'discontinuous-branched' shape has been investigated using kinetic Monte Carlo techniques [279], and it appears to be related to restricted diffusion of oxygen on the surface, which might then be related to the surface being reconstructed to the '29' or '44' structures, which are fairly corrugated (they extend up to 3.1 Å over the clean Cu(111) surface).

5.4. Island nucleation sites

A number of studies have tried to establish the role of surface defects on the nucleation of the oxide, in order to understand whether island nucleation is a heterogeneous process, triggered by specific surface features, or a homogeneous process. While some materials can grow oxide layers homogeneously without the aid of impurities or surface defects (such as Ru(0001) [261], Ag(110) [260] or Si(111) [282,283]) it has been shown that other materials, like Pb [284] or Ge(111) [285,286], cannot oxidise without the presence of surface features (impurities or defects) which trigger the dissociation of O_2 molecules.

For copper it has been shown [128,272,173,223] that defect sites play a role in oxide island nucleation. Grain boundaries [272], vacancy islands [223] and the edges of pits [271] are nucleating sites for island formation, however no preferential nucleation sites have been found at dislocations, stacking faults or impurities [271,127,272]. The importance of step edges was initially inferred by Milne and Howie [248], and the high reactivity of high-Miller index surfaces, such as Cu(410), to oxygen irradiation, seem to confirm this hypothesis [287]. Moreover, oxide formation at step edges was demonstrated on Cu (111) by means of STM and TEM [131,223]. However, TEM work [271,272] showed that island formation on Cu(100) and Cu (110) films is not affected by the presence of steps, whereas the oxide wetting layer nucleates at a step edge [173,288]. It then propagates across the terrace in an oscillatory manner, since oxygen adsorption at the lower terrace slows down the growth of the thin oxide film [274]. It is indeed possible, considering the different nature of oxide formation on the three low-index surfaces, that different defects play a more or less important role in different oxide nucleation conditions.

More work is needed to clarify further the correlation between defect sites and oxide formation and remove doubts on whether small, non-structured dislocations and impurities have a role in the nucleation of copper oxide islands, and, from a theory point of view, why some type of defects seem more efficient at nucleating oxide islands than others.

5.5. Nano-island formation kinetics

A number of models have been proposed to explain the kinetics governing the initial stages of oxide growth, from island nucleation to their coalescence. The mechanism of nucleation and initial growth of oxide islands on a clean Cu surface has been proposed in terms of 'capture zones', a well-established idea in non-homogeneous film formation theory [289,290]. In this interpretation, schematically shown in Fig. 10a, oxygen atoms within a capture zone, i.e. an area with radius L_d surrounding the island, will likely aggregate with the island and contribute to island growth rather than

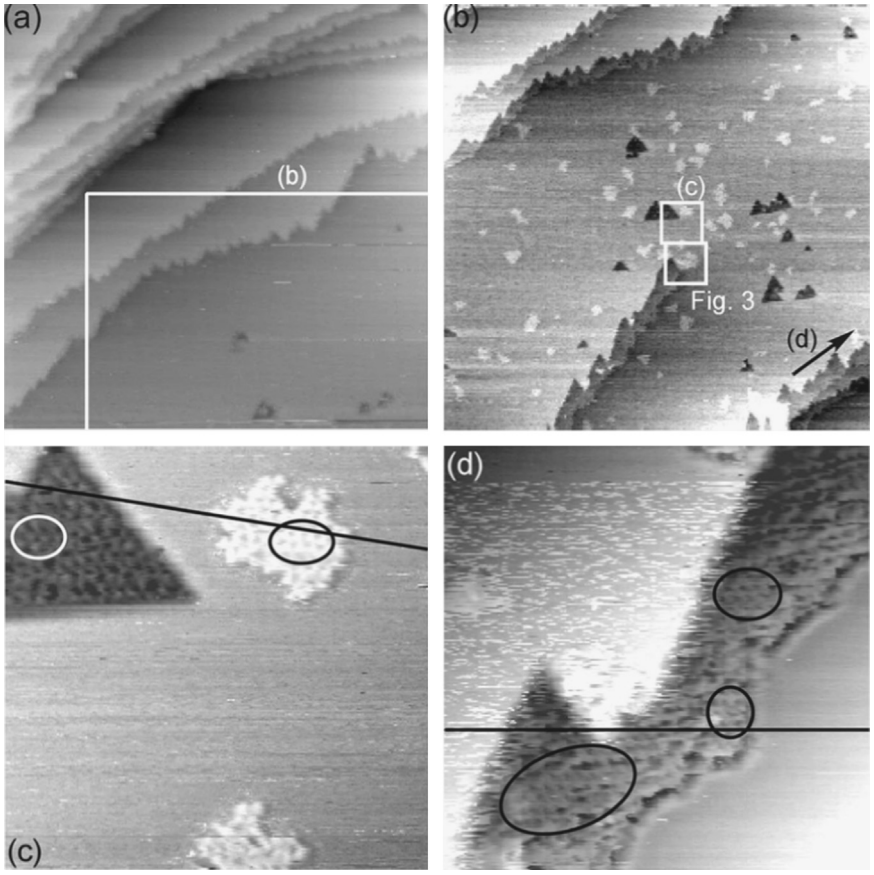

Fig. 8. Structures observed with STM by Matsumoto et al. [223] when oxidising a Cu(111) surface with step edges (visible in panel a). In-terrace and on-terrace oxides are visible in panel b, and atomically resolved in panel c. In-terrace oxide is darker and on-terrace oxide lighter than the clean copper surface. Panel d shows the oxide which grows at the edge of the terrace. The area shown in panel a and b is 2000×2000 ° AA^2, in panels c and d is 200×200 °AA^2. The square in panel a indicates part of the area shown in b. Squares and the arrow in b indicate the areas shown in c and d.

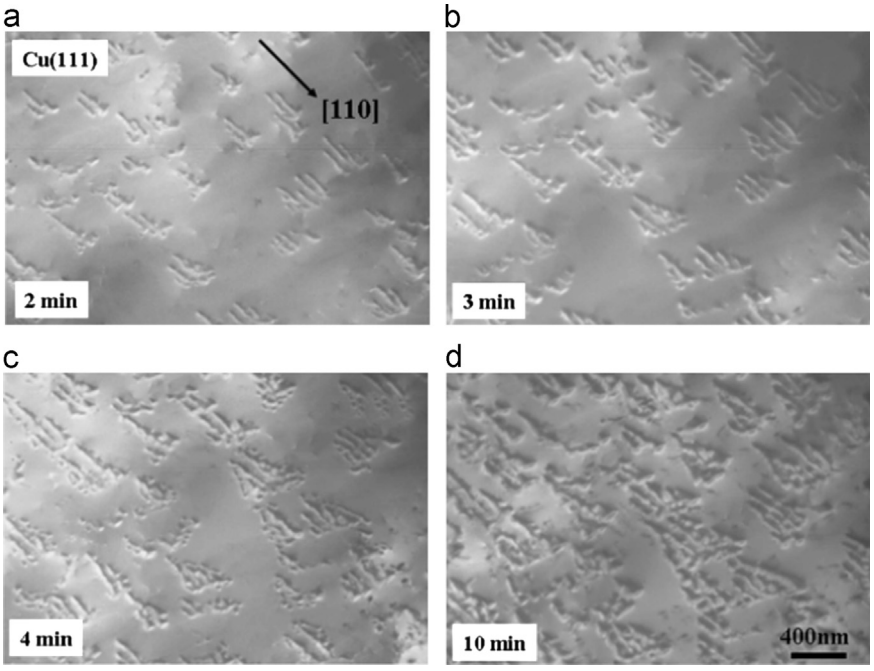

Fig. 9. Percolating oxide growth on Cu(111) observed using *in situ* TEM imaging at 450 °C. The oxidation partial pressure is $P = 5 \times 10^{-4}$ Torr. The layer is formed by preferential nucleation of islands along the [110] direction, suggesting that between 350 and 450 °C the substrate transitions from a disordered to an ordered structure. Taken from Ref. [273].

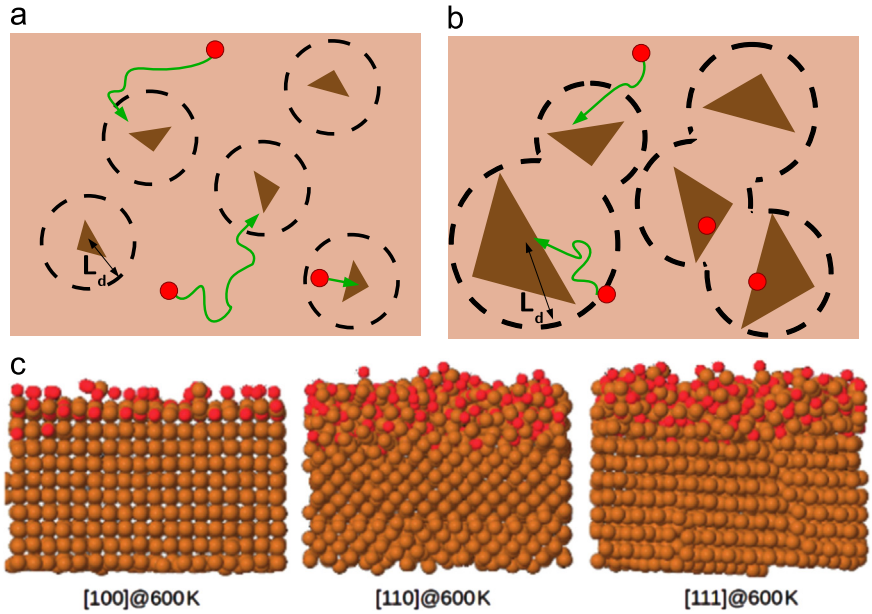

Fig. 10. (a) Schematic representation of the mechanism of island nucleation and growth according to Eq. (1). The dashed circles represent the 'oxygen capture zones' of radius L_d around the oxide islands. Oxygen atoms (in red) diffuse on the surface until they enter a capture zone, when they are incorporated in an oxide island (represented as a brown triangle). (b) Schematic representation of the mechanisms of island growth to coalescence. As the islands increase in size their areas of oxygen capture increase (black dashed line). Oxygen surface diffusion (green arrows) is still important, however direct impingement of oxygen atom on the islands is also more likely to occur. (c) Oxidation of Cu(100), Cu(110) and Cu(111) copper surfaces using the ReaxFF force field at $T = 600$ K. Cu(111) is found to oxidise more easily than (110) and (100) and form a thicker oxide film. The amorphous nature of the formed oxide is clearly visible. Taken from Ref. [296]. (For interpretation of the references to colour in this figure caption, the reader is referred to the web version of this paper.)

Table 6
Saturation density (N_{sat}), initial nucleation rate (k) and radius of the oxygen capture area (L_d) for island forming on Cu(100) and (111). Data taken from [250,259].

Surface	N_{sat} (μm^{-2})	k ($\mu m^{-2}\,min^{-1}$)	L_d (μm)
(100)	0.83	0.17	1.09
(110)	4.34	1.74	0.33

nucleating new islands. Large 'capture zones' (i.e. large values of L_d) are associated with longer path lengths of surface oxygen diffusion. In this framework, the saturation number of islands that can be nucleated, N_{sat}, is expressed as [250]

$$N_{sat} = \frac{1}{L_d^2}\left(1 - e^{-kL_d^2 t}\right), \quad (1)$$

where k is the initial island nucleation rate and t is time. This model was found to fit well experimental data for oxidation of Cu (100) and Cu(110) [250,259], as shown in Table 6. The smaller number of islands nucleating on Cu(100) is related to a larger oxygen capture area, i.e. longer path lengths for surface oxygen diffusion. This is consistent with the structure of the missing-row reconstructed Cu(100) surface, which is fairly smooth (it has a corrugation of 0.35 Å [150]), see Section 4.1, thus favouring surface diffusion. Similarly, the short diffusion path length for Cu (110) is consistent with the added-row reconstruction which protrudes ~1.5 Å over the Cu surface [159,114] (see Section 4.2). Nucleation is seen to be faster on Cu(110) than on Cu(100), see Table 6, and even faster on Cu(111) at 350 °C [273]. The O-induced reconstruction of the Cu(111) surface has been reported to have a disordered surface overlayer at room temperature, with O and Cu atoms at different heights [221,112] (see Section 4.3). This could explain a shorter path length for oxygen diffusion on Cu (111) leading to fast nucleation of a large number of oxide islands.

After island nucleation has reached saturation point, they start growing until coalescence. Island growth models based on oxygen impingement and surface diffusion (schematically represented in Fig. 10b) have been developed [291,292,249]: oxygen surface diffusion initially dominates the oxide growth, and later oxygen direct impingement becomes significant when the oxide islands grow larger in size. In particular the model proposed by Yang et al. [249] was found to fit well experimental data on Cu(100), with island growth proportional to $t^{1.3}$.

Another well established theory for the formation of thin films is the Avrami (or JMAK) nucleation model [293–295]. It presumes isotropic and homogeneous nucleation of the islands and depends exponentially on time:

$$X(t) = 1 - e^{-kt^n}, \quad (2)$$

where X is the oxide thickness. Cu(100) fits this model [259] with $k = 1.9 \times 10^{-4}$ and $n = 2$. The value of k is much smaller than expected (typically it is $k \simeq \pi/3$), possibly because of the non-constant island nucleation in cuprous oxide (but rather following the relation in Eq. (1)) and the non-linear island growth rate ($A(t) \propto t^{1.3}$). Yang et al. modified the JMAK model in order to take into account these two factors and found an excellent fit with Cu(100) experimental data [14].

Although the nucleation of islands is faster on Cu(110), the long term (> 60 min) oxidation of the (100) surface of copper

is much faster than on the (110) and (111) [280,244,246] surfaces. Fast initial nucleation and growth of islands on Cu (110) and Cu(111) leads quickly to a thinner coalesced film, which then continues growing through oxygen diffusion through the oxide layer, a much slower process than surface diffusion. On the contrary, the slow nucleation of islands on Cu(100) leads to slower coalescence to a thicker oxide film with respect to the Cu(110) and Cu(111) and thus quicker oxide growth by means of surface diffusion.

The case of oxidation on Cu(111) at higher temperatures (over 550 °C) is the only one where Cu_2O two-dimensional thin film growth is observed [273,131]. The O-induced surface reconstruction of Cu(111) at high temperatures, as seen on Section 4.3, has an hexagonal morphology similar to the Cu_2O (111) plane [221,112] which can act as a 'template' structure for the layered growth of the oxide.

A few computational studies have tried to obtain further insight into the kinetics of oxide growth, with limited success so far. The correct relative rates on the three low-index Cu surfaces have been obtained using molecular dynamics with ReaxFF, a bond order potential [296]. However the calculation led to the formation of a uniform amorphous thin film (as shown in Fig. 10c), thus not reproducing crystalline island formation as seen in experiments, and the role of the surface reconstruction was not taken into account. As already mentioned, Devine et al. [268] looked to reproduce oxidation on an O-reconstructed Cu(100) surface, using standard molecular dynamics and a bond order potential. However, the process was too slow and the simulation too short for it to be modelled.

5.6. Long-term copper oxidation

After nucleation, growth and coalescence of copper oxide islands, oxidation proceeds through the diffusion of oxygen atoms through the oxide and the character of the oxidation process changes.

The kinetics and mechanism of copper oxidation, after the exposure of the copper surface to oxygen flow for an extended period (up to 32 h) have been extensively studied [15,297,298], however no consensus on a single rate law describing the oxidation dynamics has been established.

Clean copper surfaces have been found to oxidise at different rates, with the Cu(100) face reported to have the fastest rate of oxidation, at odds with the oxidation rates measured for the formation and growth of oxide nano-islands. Indeed, Young et al. [244] and Gwathmey et al. [245] found that the order of oxidation rate for the low-index surfaces is (100), (111), (110) with (100) the fastest oxidising facet, for a wide range of temperatures. Rhodin [299] found instead the order to be (100), (110), (111). This difference in ordering could be due to several factors, for example the use of very different experimental analysis techniques. Gwathmey et al. [245] used diffuse white light to analyse the oxidised surfaces, observing different interference colours corresponding to different oxide thicknesses, Young et al. [244] used ellipsometry which relies on a 'guess' of a surface model and Rhodin [299] calculated the film thickness from weight changes in the sample. All three methods present some drawbacks (diffuse white light does not provide a value for the thickness and relies on visual checking of the surface colour, ellipsometry relies on a guess model and Rhodin's method depends on an accurate estimation of the effective area of the resulting oxide) and it is difficult to tell which of the three is more reliable. The difference observed could also be the result of environmental factors such as the presence of impurities or different sample preparations, which have been shown to lead to different resulting metal oxides [300,301] which makes oxidising metals very challenging to study.

Very large discrepancies are observed in models for oxidation rates, i.e. growth of thickness of the oxide as a function of time, and they are summarised in Fig. 11. A number of theories have been proposed [302–305], mostly based on the Cabrera–Mott [306] model. According to this theory, the (epitaxial) oxide formation process is driven, after exposure of the surface to oxygen, by an electric field produced by positive metal ions at the metal-oxide interface and negative ions at the oxide air interface. The electric fields causes the ions to migrate from the bulk to the surface, leaving metal ion vacancies in the bulk. As the oxide layer increases the electric field strength diminishes and the ion migration, and thus the film growth, slows down and eventually stops, following an inverse logarithmic rate law:

$$\frac{1}{d} = A - B \ln t \tag{3}$$

where d is the oxide film thickness, t is exposure time and A and B are fit parameters related to the metal cation formation, the electric field and the energy for diffusion across the oxide layer. This law is formulated for very thin films (up to 7.3 nm for Cu), while for thicker films (up to 1.5 μm) a cubic growth rate is expected instead. A number of works [299,307,244,308] find qualitative agreement with the Cabrera–Mott theory, however linear oxide growth has been observed in other studies [281,309,310], as well as power ($n < 1$) [311] or parabolic law [312].

Many factors can affect the experimental measurements of oxide kinetics, such as the environment and the type of initial copper sample. Indeed, it was found that polycrystalline film oxidation kinetics is almost twice as slow as single crystal oxidation kinetics, for films of equal thickness under the same conditions [313,310]. The oxidation temperature is another factor [314–316]. O'Reilly et al. [315] found that, for a polycrystalline sample in dry synthetic air (O_2/Ar mixture), between 250–500°C the oxidation followed a cubic law, at 100 °C an inverse log rate and at 150 °C a linear growth rate. Gao et al. [316] found a linear oxidation rate between 200–250 °C with a fine-grained Cu_2O being the resultant oxide, and parabolic above that, with CuO the final oxidation product.

Although a lot of work has been performed in this field, it is clear from Fig. 11 that there is no consistency in the results obtained. Systematic work under well defined conditions looking at the influence of crystal structure (single crystal, polycrystalline, different grain sizes), experimental set-up (humidity, temperature, oxygen pressure) and composition of

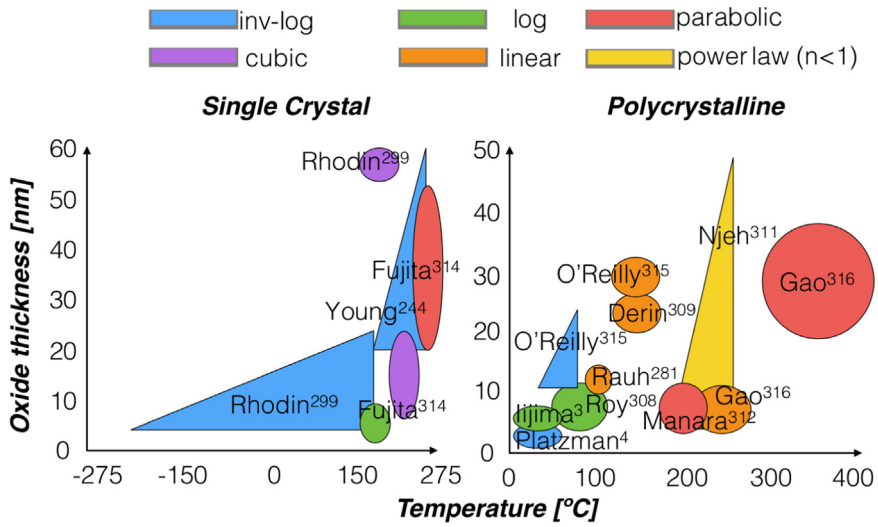

Fig. 11. Overview of growth models for copper oxide present in the literature. The graphs show the oxide film thickness *vs* oxidation temperature for a number of experimental studies. The data is divided into two categories, according to the composition of the initial copper sample, single crystal or polycrystalline. They have also been colour coded according to the oxidation kinetic model which has been attributed to them. It can be seen that on the basis of these three parameters only (temperature, film thickness and initial sample structure) a single kinetic model cannot be identified. (For interpretation of the references to colour in this figure caption, the reader is referred to the web version of this paper.)

the oxide product are needed in order to clarify where the contributions to these different oxidation rates originate from.

5.7. Native oxidation of copper in ambient conditions

Structural details of the room temperature oxidation of copper under ambient conditions, including the possible influence of humidity and crystal structure, are not very clear.

In order to study copper in ambient conditions (room-temperature, 1 atm pressure) precise measurement techniques are required, since surface oxide films are generally only a few nm thick. Experiments studying oxidation in these conditions have been performed for an enormous range of exposure times, between 30 min and 9 months, in air at ambient conditions (referred to as ambient air hereafter), obtaining results which are not always consistent (see Table 7). As we will see, the outcome of the studies differs in the thickness of the final oxide, in the presence or not of a CuO overlayer on top of the Cu_2O oxide layer and in the order of formation of the oxides. The reason for this non-uniformity is probably to be found in the method of preparation of the film, on the type of film used (thin/bulk, polycrystalline/single crystal), the ambient humidity (which is rarely reported) and the surface roughness.

Native oxidation has been extensively studied, by means of XAS, XPS (to identify the composition) and ellipsometry (to measure the film thickness), in copper thin films (a few hundred nms-thick). This is mainly because of the technological impact of the formation of thin oxide layers in the passivation of nano-sized electronic copper parts. Platzman et al. [4] proposed a three-stage oxidation mechanism involving: (a) the formation of a Cu_2O layer following a Cabrera–Mott model; (b) the formation of a $Cu(OH)_2$ metastable overlayer, due to the interaction of Cu ions with hydroxyl groups present at the surface; and (c) the transformation of the metastable $Cu(OH)_2$ phase to a more stable CuO layer. Indeed, the formation of a ~2.0–5.0 nm Cu_2O layer first, followed by a ~0.9–1.3 nm CuO overlayer has been reported [4,3,317–319,319]. However, Lim et al. [301] showed that the texture and microstructure of a thin copper film have a direct influence on the oxidation products. When oxidising a sample with a columnar structure and small grains the Cu_2O/CuO bilayer was obtained, when oxidising a uniform sample with no obvious columnar structure and grain boundaries the cuprous oxide layer only was observed and oxidation was slower.

The oxidation of bulk copper was studied by means of XPS, XRD and ellipsometry, and the results obtained are mixed. A number of studies [3,320,321] found only the formation of ~1.6 nm thick Cu_2O even after long exposure times. However, other studies of passivated Cu after exposure to air at room temperature [2,322] observed the formation of thin CuO film, which was found to start growing only after the Cu_2O growth process had finished. The different results obtained by these experiments can be due to the texture and microstructure of the copper film [301], by the surface roughness or by defects present at the surface. Indeed, the surface roughness of metal oxide surfaces has been shown to have a direct influence on their wetting properties towards water, which in turn could have a direct influence on the formation of the native oxide [323]. In particular, very smooth copper surfaces are hydrophobic while rough surfaces (~5 nm-high roughness) are hydrophilic [324]. Furthermore the orientation of the crystallites at the surface influences the wetting properties and the distribution and coverage of water on the surface, especially in the case of copper [325]. Moreover, polycrystalline structures with nanosized grains have higher surface energy at the grain boundaries than structures that are made of micrometric grains of crystalline lattice, which in turn affect the wettability of the surface.

Table 7
Summary of experimental studies on the native oxidation of copper. Details of the sample type, preparation and environmental conditions have been specified, together with the experimental techniques used and the observed oxide structure.

Author	Sample	Environment	Surface treatment	Exposure time	Technique	Resulting oxide structure
Barr [2] (1978)	Commercial film	RT air, 35% humidity	Sputter etching	30 min-days	ESCA	2.0 nm Cu_2O/CuO or 2.0 nm Cu_2O
Chawla [320] (1992)	Commercial film	Air	Electropolishing	24 h in a desiccator	XPS	1.6 nm Cu_2O
O'Reilly [315] (1995)	Bulk (2 mm), film (80–500 nm)	$T = 50$–150 °C, dry synthetic air	Bulk: ground surfaces. Film: electroless deposition, sputtering	300 min	TGA, XRD	$T < 100$ °C: Cu_2O, $T > 100$ °C: Cu_2O and CuO
Suzuki [322] (1997)	0.5 mm	RT air	Electrolytical polishing	10 min-1 2 days	XPS	2^+ and 1^+ oxidation states present
Chu [321] (1999)	Commercial film	RT air and aqueous solution	Electropolishing	23 h	XRD	Cu_2O
Iijima [3] (2006)	Cu bulk 0.5 mm and Cu film	RT air	Electrochemical polishing, annealing in dry H at 600°	30 min-1300 h	XPS, ellipsometry	Cu_2O on Cu bulk, Cu_2O/CuO on Cu film
Lim [301] (2008)	100 nm	RT air, 10% humidity	ion beam deposition, argon ion sputtering	30 min-1280 h	XPS, SEM, HRTEM	Cu deposited with 0 V bias voltage at the substrate shows both Cu_2O and CuO, with −50 V only Cu_2O
Platzman [4] (2008)	~400 nm	RT air, 60% humidity	Thermal filament evaporation deposition on Si wafers.	1 h-112 days	XPS, TEM, SEM	After 1 h only Cu_2O observed, CuO starts occurring after 24 h
Keil [318,317] (2010)	90 nm	RT air	DC sputtering on glass	48 h-9 months	XAS	Oxide bilayer: 2.0 nm CuO over 3.5 nm Cu_2O
Chen [326] (2013)	Commercial film	Heated to $T = 200$–800 °C in air	Cleaning with absolute alcohol and deionised water	~10 h	FESEM, XRD	Cu_2O/CuO oxide bilayer
Zuo [319] (2014)	Commercial film	UHV and RT air (20% humidity)	Ar^+ sputtering	1800 h	XPS	Cu_2O/CuO oxide bilayer in air

5.8. CuO formation

CuO is expected to form after exposure of a copper surface to oxygen at high temperatures and pressure [39,241]. Much work has gone into understanding high temperature oxidation of copper (>350°) and it has been recently reviewed [327,328]. Most work shows the growth of CuO on top of Cu_2O, following a parabolic rate law for the thickness as a function of time. However, no studies of the atomistic details of the formation of CuO at high temperatures have been performed to date.

As already shown is Section 5.7, growth of a CuO layer over a thicker Cu_2O one has been observed for long-term copper oxidation in ambient air. Similarly, in controlled conditions, evidence of a CuO overlayer was found by exposing a Cu sample to a controlled flow of O_2 at high pressure and the dependence of oxidation on oxygen pressure was analysed. Boggio [329] investigated the pressure dependence ($P = 0.03$–7.5 Torr) on the oxidation of Cu(111), and in particular the film thickness, using ellipsometry. The film growth (thought to be Cu_2O), after 90 min exposure at 21°, was related to the Cabrera–Mott expression of growth. However, a dramatic decrease in the oxidation rate with increased oxygen pressure was observed and related to the formation of a passivating CuO film at the oxide-oxygen interface. Pierson et al. [242] looked at the reactivity of a number of noble metals when subject to a flow of gases. In the case of Cu in an O_2 flow, the formation of oxidised structures was found to depend on the flow rate of O_2. The formation of Cu_2O (at oxygen partial pressure $P = 7.5 \times 10^{-5}$ Torr), CuO ($P = 1.12 \times 10^{-3}$ Torr) and metastable Cu_4O_3 ($P = 1.5 \times 10^{-4}$ Torr), was observed by XRD analysis.

6. Conclusion and discussion

The oxidation of copper and the physical properties of the resulting oxides are fundamental scientific problems which are still not completely understood today. Since there has currently been a surge of interest in the use of copper oxide for catalysis, optoelectronics and gas sensing, the need for a detailed understanding of the surface structures of these oxides has become even more pressing. In addition, uncontrolled copper oxidation is still an issue in *e.g.* electronic applications, and understanding the oxide growth process is the first step towards mitigating it.

In this review we have discussed the state of the knowledge regarding the structure and formation of copper oxides and we have seen that the structural, optic and vibrational characteristics of bulk copper oxides are well understood. A good amount of computational work (mainly from DFT) has been performed on both Cu_2O and CuO, providing important information on the structures of the surfaces at different

temperature and pressure conditions. A (111) surface with hexagonal symmetry and presenting Cu surface vacancies was found to be the most stable on Cu_2O. The stoichiometric (111) surface is the most stable for CuO. Few experimental studies are available to either confirm or disprove these suggestions from theory. Considering the potential technological applications of these oxides, this is an area which should be looked at more with experimental techniques such as STM, XPS or LEED (most likely with the oxides supported by metallic substrates).

Many atomistic aspects of the formation of the oxides have been established. Indeed, the oxygen-induced surface reconstructions on copper surfaces with low Miller index are well known. Moreover, recent STM studies have revealed additional atomic level details of the initial stages of Cu surface oxidation. AFM and STM work at low oxygen pressure has also shown that the initial oxide growth happens through the formation of cuprous oxide islands which eventually coalesce. The kinetics of oxide formation depends on the temperature and on the structure of the copper surface and it is dominated by oxygen surface diffusion and direct impingement in the first instance, and after coalescence by oxygen diffusion into the bulk.

There is however scope for further work as many fundamental aspects of copper oxidation are still unclear. In fact, there is no consensus on how the transition from an oxygen-reconstructed copper surface to an oxidised one occurs, whether this is after the surface has entirely reconstructed or if the islands start forming on the clean surface. At least for the case of Cu(100) and Cu(110), there is good evidence that the onset of oxidation will occur after the formation of an O-reconstructed overlayer which affects the growth kinetics of the islands themselves. The precise understanding of the formation of these copper islands is not only important to understand the onset of oxidation, but also to exploit the oxide islands as nano-templates for technological applications. In order to do that the precise mechanism of nucleation needs to be understood.

It is also unclear where the different behaviour between metals such as Ag or Al, which grow uniform oxide layers, and copper stems from. The O-induced surface reconstructions of different fcc metals have been extensively studied [114] and the differences found in their electronic structures [330] or surface configurations [331] could provide hints to their different behaviour upon higher exposure to oxygen. The incorporation of subsurface oxygen into various metals has also been considered with DFT [332], however, dedicated theoretical studies on this issue have not yet been performed on copper.

The kinetics of long-term oxide growth, both in controlled conditions and in ambient air, is an issue that remains poorly understood. Copper oxide formation does not simply follow the Cabrera–Mott law, especially at the initial stages when oxide growth is not uniform across the surface. Many studies have been performed in order to establish the oxide formation kinetics at low temperatures, however they are difficult to compare to one another, because of the different conditions in use. Indeed temperature, humidity, oxygen partial pressure, structure of the initial copper film/coupon, the presence of defects and impurities seem to affect the growth of the oxide as well as the final oxide product. Moreover, the structure of copper oxide when grown in ambient air, which is very important to the practical uses of copper, is still not clearly understood, with the formation of a CuO overlayer on top of a Cu_2O layer still being debated. Further systematic experimental studies, looking at disentangling the environmental factors influencing oxide growth are needed. Computationally, additional studies of copper and copper oxide surfaces and their interaction with the environment (*e.g.* water, O_2, N_2) would provide valuable information in support of the experimental work. Work in this direction has recently been reported, *e.g.* water and hydroxide adsorption on Cu and Cu oxide [333–336,207].

Partly the challenges in studying these systems arise from limitations of theoretical and experimental techniques. It is indeed clear that massive steps forward have been made since the first calorimetry experiments on Cu_2O crystals, and nanometre scale resolution or better has been obtained with STM, TEM and LEED. Moreover, the development of experimental techniques, such as X-ray lasers with extremely high spatial and temporal resolution [337] or near-ambient pressure photoelectron spectroscopy [338,339] or STM [340,341], might enable the mechanisms of initial stages of oxidation to be explored.

Computational techniques also present challenges from the point of view of accuracy of calculated structures and physical properties [31,205], as well as simulation length when considering molecular dynamics. Moreover developments in theory, especially *ab initio* molecular dynamics, accelerated sampling techniques and more sophisticated non-*ab initio* approaches mean that similar studies on the first steps of oxidation are possible. *Ab initio* molecular dynamics, along with a free energy sampling approach, has been used to examine the initial stages of NaCl dissolution in liquid water [342]: it is not inconceivable that similar techniques could be applied to copper oxidation in ambient and even aqueous conditions.

Finally, another important challenge is bridging the gap between highly controlled studies performed in ultra-high vacuum and work aiming to understand the formation of the oxide in industrially relevant conditions. At the moment, these two aspects of the oxidation problem are addressed using different techniques at different resolutions. In order to fully understand the oxidation of copper it is important to be able to relate the results obtained in these different conditions to one another and build a unified picture of the problem.

Acknowledgements

A.M.'s work is partly supported by the European Research Council under the European Union's Seventh Framework Programme (FP/2007-2013)/ERC Grant Agreement no. 616 121 (HeteroIce project) and the Royal Society through a Wolfson Research Merit Award.

References

[1] M. Miodownik, Stuff Matters: The Strange Stories of the Marvellous Materials that Shape Our Man-made World, Penguin, London, 2014.
[2] T.L. Barr, J. Vac. Sci. Technol. 14 (1977) 660.
[3] J. Iijima, J.W. Lim, S.H. Hong, S. Suzuki, K. Mimura, A. Isshiki, Appl. Surf. Sci. 253 (2006) 2825.
[4] I. Platzman, R. Brener, H. Haick, R. Tannenbaum, J. Phys. Chem. C 112 (2008) 1101.
[5] J. Song, L.L. Wang, A. Zibart, C. Koch, Metals 2 (2012) 450.
[6] P. Szakalos, G. Hultquist, G. Wikmark, Electrochem. Solid State 10 (2007) C63.
[7] J.B. Reitz, E.I. Solomon, J. Am. Chem. Soc. 120 (1998) 11467.
[8] Y. Nakamura, H. Yoshioka, M. Miyayama, H. Yanagida, T. Tsurutani, Y. Nakamura, J. Electrochem. Soc. 137 (1990) 940.
[9] B. Rai, Sol. Cells 25 (1988) 265.
[10] B.K. Meyer, A. Polity, D. Reppin, B. Becker, P. Hering, P.J Klar, T. Sander, C. Reindl, J. Benz, M. Eickhoff, C. Heiliger, M. Heinemann, J. Blaesing, A. Krost, S. Shokovets, C. Mueller, C. Ronning, Phys. Status Solidi B 249 (2012) 1487.
[11] M.S. Hunter, P. Fowle, J. Electrochem. Soc. 103 (1956) 482.
[12] H. Lu, E. Gusev, E. Garfunkel, T. Gustafsson, Surf. Sci. 351 (1996) 111.
[13] C. Palacio, H.J. Mathieu, Surf. Interface Anal. 16 (1990) 178.
[14] J.C. Yang, D. Evan, L. Tropia, Appl. Phys. Lett. 81 (2002) 241.
[15] K.R. Lawless, Rep. Prog. Phys. 37 (1974) 231.
[16] H.J. Freund, H. Kuhlenbeck, V. Staemmler, Rep. Prog. Phys. 59 (1996) 283.
[17] U. Diebold, S.-C. Li, M. Schmid, in: S. Leone, P. Cremer, J. Groves, M. Johnson, G. Richmond (Eds.), Annual Review of Physical Chemistry, Annual Reviews, vol. 61, , 2010, p. 129.
[18] G.A. Somorjai, Introduction to Surface Chemistry and Catalysis, A Wiley-Interscience Publication, Wiley, New York, 1994.
[19] A. Gross, Theoretical Surface Science: A Microscopic Perspective; with 11 Tables and 32 Exercises, Advanced Texts in Physics, Springer, Berlin, Heidelberg, 2003.
[20] K. Wandelt, Surface and Interface Science, Wiley, Weinheim, 2012.
[21] G. Bracco, B. Holst, Surface Science Techniques, Springer Series in Surface Science, Springer, Berlin, Heidelberg, 2013.
[22] M. Salmeron, R. Schlögl, Surf. Sci. Rep. 63 (2007) 169.
[23] J. Behler, Coarse-grained Electronic Structure using Neural Networks, in: J. Grotendorst, N. Attig, S. Bluegel, D. Marx (Eds.), Multiscale simulation methods in molecular sciences, NIC Series, vol. 42, Julich Supercomputing Centre, 2009, p. 247.
[24] W.J. Szlachta, A.P. Bartók, G. Csányi, Phys. Rev. B 90 (2014) 104108.
[25] A.C.T. van Duin, S. Dasgupta, F. Lorant, W.A. Goddard, J. Phys. Chem. A 105 (2001) 9396.
[26] A. Warshel, M. Levitt, J. Mol. Biol. 103 (1976) 227.
[27] W. Kohn, L.J. Sham, Phys. Rev. 140 (1965) A1133.
[28] P. Hohenberg, W. Kohn, Phys. Rev. 136 (1964) B864.
[29] V. Brazdova, D.R. Bowler, Atomistic Computer Simulations: A Practical Guide, Wiley, Weinheim, 2013.
[30] S. Curtarolo, G.L.W. Hart, M.B. Nardelli, N. Mingo, S. Sanvito, O. Levy, Nat. Mater. 12 (2013) 191.
[31] K. Burke, J. Chem. Phys. 136 (2012) 150901.
[32] B. Himmetoglu, A. Floris, S. de Gironcoli, M. Cococcioni, Int. J. Quantum Chem. 114 (2014) 14.
[33] J.P. Perdew, A. Zunger, Phys. Rev. B 23 (1981) 5048.
[34] J. Heyd, G.E. Scuseria, M. Ernzerhof, J. Chem. Phys. 118 (2003) 8207.
[35] C. Adamo, V. Barone, J. Chem. Phys. 110 (2005) 6158.
[36] F. Aryasetiawan, O. Gunnarsson, Rep. Prog. Phys. 61 (1998) 237.
[37] J.C. Slater, Phys. Rev. 35 (1930) 210.
[38] J.C. Slater, G.F. Koster, Phys. Rev. 94 (1954) 1498.
[39] G. Honjo, J. Phys. Soc. Jpn. 4 (1949) 330.
[40] S.P. Tandon, J.P. Gupta, Phys. Status Solidi 37 (1970) 43.
[41] J. Ghijsen, L.H. Tjeng, J. Vanelp, H. Eskes, J. Westerink, G.A. Sawatzky, M.T. Czyzyk, Phys. Rev. B 38 (1988) 11322.
[42] K.P. Bohnen, R. Heid, L. Pintschovius, A. Soon, C. Stampfl, Phys. Rev. B 80 (2009) 134304.
[43] R. Mittal, S.L. Chaplot, S.K. Mishra, P.P. Bose, Phys. Rev. B 75 (2007) 174303.
[44] A. Hallil, J.-M. Raulot, M. Cherkaoui, Comput. Mater. Sci. 81 (2014) 366.
[45] J. Robertson, Phys. Rev. B 28 (1983) 3378.
[46] A. Sanson, Solid State Commun. 151 (2011) 1452.
[47] M.M. Islam, B. Diawara, V. Maurice, P. Marcus, J. Mol. Struc.-Theochem. 903 (2009) 41.
[48] A. Martinez-Ruiz, M.G. Moreno, N. Takeuchi, Solid State Sci. 5 (2003) 291.
[49] A. Soon, M. Todorova, B. Delley, C. Stampfl, Phys. Rev. B 73 (2006) 165424.
[50] E. Ruiz, S. Alvarez, P. Alemany, R.A. Evarestov, Phys. Rev. B 56 (1997) 7189.
[51] H. Raebiger, S. Lany, A. Zunger, Phys. Rev. B 76 (2007) 045209.
[52] R. Laskowski, P. Blaha, K. Schwarz, Phys. Rev. B 67 (2003) 8.
[53] A. Filippetti, V. Fiorentini, Phys. Rev. B 72 (2005) 8.
[54] A. Onsten, M. Gothelid, U.O. Karlsson, Surf. Sci. 603 (2) (2009) 257.
[55] J.P. Hu, D.J. Payne, R.G. Egdell, P.A. Glans, T. Learmonth, K.E. Smith, J. Guo, N.M. GHarrison, Phys. Rev. B 77 (2008) 155115.
[56] M. van Schilfgaarde, T. Kotani, S. Faleev, Phys. Rev. Lett. 96 (2006) 226402.
[57] P. Cortona, M. Mebarki, J. Phys. Condens. Matter 23 (2011) 8.
[58] A.B. Gordienko, Y.N. Zhuravlev, D.G. Fedorov, Phys. Solid State 49 (2007) 223.
[59] X.L. Nie, S.H. Wei, S.B. Zhang, Phys. Rev. B 65 (2002) 075111.
[60] M. Heinemann, B. Eifert, C. Heiliger, Phys. Rev. B 87 (2013) 5.
[61] F. Tran, P. Blaha, Phys. Rev. B 83 (2011) 235118.
[62] L.Y. Isseroff, E.A. Carter, Phys. Rev. B 85 (2012) 235142.
[63] D. Le, S. Stolbov, T.S. Rahman, Surf. Sci. 603 (2009) 1637.
[64] A. Soon, T. Sohnel, H. Idriss, Surf. Sci. 579 (2005) 131.
[65] D.O. Scanlon, B.J. Morgan, G.W. Watson, A. Walsh, Phys. Rev. Lett. 103 (2009) 096405.
[66] F. Bruneval, N. Vast, L. Reining, M. Izquierdo, F. Sirotti, N. Barrett, Phys. Rev. Lett. 97 (2006) 4.
[67] T. Kotani, M. van Schilfgaarde, S.V. Faleev, Phys. Rev. B 76 (2007) 165106.
[68] S. Lany, Phys. Rev. B 87 (2013) 085112.
[69] C. Noguera, J. Phys. Condens. Matter 12 (2000) R367.
[70] K.H. Schulz, D.F. Cox, Phys. Rev. B 43 (1991) 1610.
[71] M.M. Islam, B. Diawara, V. Maurice, P. Marcus, Surf. Sci. 604 (2010) 1516.
[72] M.A. Nygren, L.G.M. Pettersson, A. Freitag, V. Staemmler, D.H. Gay, A.L. Rohl, J. Phys. Chem. 100 (1996) 294.
[73] N.D. McClenaghan, P.J. Hu, C. Hardacre, Surf. Sci. 464 (2000) 223.
[74] M.M. Islam, B. Diawara, P. Marcus, Surf. Sci. 603 (2009) 2087.
[75] M. Li, J.Y. Zhang, Y. Zhang, G.F. Zhang, T.M. Wang, Appl. Surf. Sci. 257 (2011) 10710.
[76] C. Li, F. Wang, S.F. Li, Q. Sun, Y. Jia, Phys. Lett. A 374 (2010) 2994.
[77] A. Soon, M. Todorova, B. Delley, C. Stampfl, Phys. Rev. B 75 (2007) 125420.
[78] A. Soon, M. Todorova, B. Delley, C. Stampfi, Surf. Sci. 601 (2007) 5809.
[79] K. Reuter, M. Scheffler, Phys. Rev. B 65 (2002) 035406.
[80] A.T. Lozovoi, A. Alavi, M.W. Finnis, Comput. Phys. Comm. 137 (2001) 174.
[81] S. Asbrink, L.J. Norrby, Acta Crystallogr. B 26 (1970) 8.
[82] S.C. Ray, Sol. Energy Mater. Sol. Cells 68 (2001) 307.
[83] K.L. Hardee, A.J. Bard, J. Electrochem. Soc. 124 (1977) 215.
[84] F.P. Koffyberg, F.A. Benko, J. Appl. Phys. 53 (1982) 1173.
[85] F. Marabelli, G.B. Parravicini, F. Salghettidrioli, Phys. Rev. B 52 (1995) 1433.
[86] J.B. Forsyth, P.J. Brown, B.M. Wanklyn, J. Phys. C 21 (1988) 2917.
[87] B.X. Yang, J.M. Tranquada, G. Shirane, Phys. Rev. B 38 (1988) 174.
[88] P.J. Brown, T. Chattopadhyay, J.B. Forsyth, V. Nunez, F. Tasset, J. Phys. Condens. Matter 3 (1991) 4281.

[89] M. Ain, A. Menelle, B.M. Wanklyn, E.F. Bertaut, J. Phys. Condens. Matter 4 (1992) 5327.
[90] Y. Peng, Z. Zhang, T.V. Pham, Y. Zhao, P. Wu, J.L. Wang, J. Appl. Phys. 111 (2012) 5.
[91] L. Debbichi, M.C.M. de Lucas, J.F. Pierson, P. Kruger, J. Phys. Chem. C 116 (2012) 10232.
[92] J. Hu, D.D. Li, J.G. Lu, R.Q. Wu, J. Phys. Chem. C 114 (2010) 17120.
[93] D.X. Wu, Q.M. Zhang, M. Tao, Phys. Rev. B 73 (2006) 6.
[94] W. Reichardt, F. Gompf, M. Ain, B.M. Wanklyn, Z. Phys. B 81 (1990) 19.
[95] M.A. Dar, Q. Ahsanulhaq, Y.S. Kim, J.M. Sohn, W.B. Kim, H. Shin, Appl. Surf. Sci. 255 (2009) 6279.
[96] X.K. Chen, J.C. Irwin, J.P. Franck, Phys. Rev. B 52 (1995) 13130.
[97] G. Kliche, Z.V. Popovic, Phys. Rev. B 42 (1990) 10060.
[98] V.I. Anisimov, J. Zaanen, O.K. Andersen, Phys. Rev. B 44 (1991) 943.
[99] C.E. Ekuma, V.I. Anisimov, M. Jarrell, J. Moreno, Eur. Phys. J. B 87 (2014) 23.
[100] P. Jiang, D. Prendergast, F. Borondics, S. Porsgaard, L. Giovanetti, E. Pach, J. Newberg, H. Bluhm, F. Besenbacher, M. Salmeron, J. Chem. Phys. 138 (2013) 024704.
[101] M. Nolan, S.D. Elliott, Phys. Chem. Chem. Phys. 8 (2006) 5350.
[102] A. Svane, O. Gunnarsson, Phys. Rev. Lett. 65 (1990) 1148.
[103] Z. Szotek, W.M. Temmerman, H. Winter, Phys. Rev. B 47 (1993) 4029.
[104] A. Filippetti, V. Fiorentini, Phys. Rev. Lett. 95 (2005) 086405.
[105] C. Rödl, F. Sottile, L. Reining, Phys. Rev. B 91 (2015) 045102.
[106] J.F. Pierson, A. Thobor-Keck, A. Billard, Appl. Surf. Sci. 210 (2003) 359.
[107] S.L. Dudarev, G.A. Botton, S.Y. Savrasov, C.J. Humphreys, A.P. Sutton, Phys. Rev. B 57 (1998) 1505.
[108] Q. Zhang, K. Zhang, D. Xu, G. Yang, H. Huang, F. Nie, C. Liu, S. Yang, Prog. Mater. Sci. 60 (2014) 208.
[109] S. Warren, W.R. Flavell, A.G. Thomas, J. Hollingworth, P.L. Wincott, A.F. Prime, S. Downes, C.K. Chen, J. Phys. Condens. Matter 11 (1999) 5021.
[110] Y. Maimaiti, M. Nolan, S.D. Elliott, Phys. Chem. Chem. Phys. 16 (2014) 3036.
[111] M. Monte, D. Gamarra, A. Lopez Camara, S.B. Rasmussen, N. Gyorffy, Z. Schay, A. Martinez-Arias, J.C. Conesa, Catal. Today 229 (2014) 104.
[112] F. Jensen, F. Besenbacher, I. Stensgaard, Surf. Sci. 269 (1992) 400.
[113] S.M. Johnston, A. Mulligan, V. Dhanak, M. Kadodwala, Surf. Sci. 519 (2002) 57.
[114] F. Besenbacher, J.K. Nørskov, Prog. Surf. Sci. 44 (1993) 5.
[115] M.A. van Daelen, M. Neurock, R.A. van Santen, Surf. Sci. 417 (1998) 247.
[116] S.Y. Liem, J.H.R. Clarke, G. Kresse, Surf. Sci. 459 (2000) 104.
[117] J.-Y. Ge, J. Dai, J.Z.H. Zhang, J. Phys. Chem. 100 (1996) 11432.
[118] A. Hodgson, A.K. Lewin, A. Nesbitt, Surf. Sci. 293 (1993) 211.
[119] P. Pudney, M. Bowker, Chem. Phys. Lett. 171 (1990) 373.
[120] Y. Xu, M. Mavrikakis, Surf. Sci. 494 (2001) 131.
[121] S. Lopez-Moreno, A.H. Romero, J. Chem. Phys. 142 (2015) 154702.
[122] F. Habraken, E. Kieffer, G. Bootsma, Surf. Sci. 83 (1979) 45.
[123] B.G. Briner, M. Doering, H.P. Rust, A.M. Bradshaw, Phys. Rev. Lett. 78 (1997) 1516.
[124] T. Yokoyama, D. Arvanitis, T. Lederer, M. Tischer, L. Troger, K. Baberschke, G. Comelli, Phys. Rev. B 48 (1993) 15405.
[125] T. Sueyoshi, T. Sasaki, Y. Iwasawa, Surf. Sci. 365 (1996) 310.
[126] Z. Crljen, P. Lazic, D. Sokcevic, R. Brako, Phys. Rev. B 68 (2003) 195411.
[127] K. Heinemann, D.B. Rao, D.L. Douglass, Oxid. Met. 9 (1975) 379.
[128] L.H. Dubois, Surf. Sci. 119 (1982) 399.
[129] J.C. Yang, M. Yeadon, B. Kolasa, J.M. Gibson, Microsc. Microanal. 4 (1998) 334.
[130] K. Lahtonen, M. Hirsimaki, M. Lampimaki, M. Valden, J. Chem. Phys. 129 (2008) 124703.
[131] C.P. Leon, C. Surgers, H. von Lohneysen, Phys. Rev. B 85 (2012) 035434.
[132] M. Lee, A.J.H. McGaughey, Phys. Rev. B 83 (2011) 165447.
[133] G.W. Zhou, L. Luo, L. Li, J. Ciston, E.A. Stach, J.C. Yang, Phys. Rev. Lett. 109 (2012) 235502.
[134] P.J. Rous, Surface crystallography: the experimental date base, in: F. de Boer, D. Pettifor (Eds.), Cohesion and Structure of Surfaces, Cohesion and Structure, vol. 4, North-Holland, Amsterdam, 1995 (Chapter I).
[135] C.Q. Sun, Surf. Rev. Lett. 8 (2001) 367.
[136] T. Lederer, D. Arvanitis, G. Comelli, L. Troger, K. Baberschke, Phys. Rev. B 48 (1993) 15390.
[137] M. Alatalo, S. Jaatinen, P. Salo, K. Laasonen, Phys. Rev. B 70 (2004) 6.
[138] W.K. Chen, C.H. Lu, Z.H. Chen, Y. Li, J.Q. Li, Chin. J. Chem. Phys. 19 (2006) 54.
[139] X. Duan, O. Warschkow, A. Soon, B. Delley, C. Stampfl, Phys. Rev. B 81 (2010) 075430.
[140] K. Yagyu, X. Liu, Y. Yoshimoto, K. Nakatsuji, F. Komori, J. Phys. Chem. C 113 (2009) 5541.
[141] A. Puisto, H. Pitkanen, M. Alatalo, S. Jaatinen, P. Salo, A.S. Foster, T. Kangas, K. Laasonen, Catal. Today 100 (2005) 403.
[142] M.K. Rajumon, K. Prabhakaran, C.N.R. Rao, Surf. Sci. 233 (1990) L237.
[143] A. Spitzer, H. Luth, Surf. Sci. 118 (1982) 136.
[144] T. Katayama, D. Sekiba, K. Mukai, Y. Yamashita, F. Komori, J. Yoshinobu, J. Phys. Chem. C 111 (2007) 15059.
[145] T. Fujita, Y. Okawa, Y. Matsumoto, K. Tanaka, Phys. Rev. B 54 (1996) 2167.
[146] D. Arvanitis, G. Comelli, T. Lederer, H. Rabus, K. Baberschke, Chem. Phys. Lett. 211 (1993) 53.
[147] M. Sotto, Surf. Sci. 260 (1992) 235.
[148] M. Kittel, M. Polcik, R. Terborg, J.T. Hoeft, P. Baumgartel, A.M. Bradshaw, R.L. Toomes, J.H. Kang, D.P. Woodruff, M. Pascal, C.L.A. Lamont, E. Rotenberg, Surf. Sci. 470 (2001) 311.
[149] H.C. Zeng, R.A. Mcfarlane, K.A.R. Mitchell, Surf. Sci. 208 (1989) L7.
[150] F. Jensen, F. Besenbacher, E. Laegsgaard, I. Stensgaard, Phys. Rev. B 42 (1990) 9206.
[151] C. Woll, R.J. Wilson, S. Chiang, H.C. Zeng, K.A.R. Mitchell, Phys. Rev. B 42 (1990) 11926.
[152] F.M. Leibsle, Surf. Sci. 337 (1995) 51.
[153] M. Yata, H. Rouch, K. Nakamura, Phys. Rev. B 56 (1997) 10579.
[154] M. Wuttig, R. Franchy, H. Ibach, Surf. Sci. 213 (1989) 103.
[155] M. Wuttig, R. Franchy, H. Ibach, Surf. Sci. 224 (1989) L979.
[156] I.K. Robinson, E. Vlieg, S. Ferrer, Phys. Rev. B 42 (1990) 6954.
[157] W. Liu, K.C. Wong, H.C. Zeng, K.A.R. Mitchell, Prog. Surf. Sci. 50 (1995) 247.
[158] N. Bonini, A. Kokalj, A. Dal Corso, S. de Gironcoli, S. Baroni, Surf. Sci. 600 (2006) 5074.
[159] K. Tanaka, Y. Matsumoto, T. Fujita, Y. Okawa, Appl. Surf. Sci. 130 (1998) 475.
[160] H. Iddir, D.D. Fong, P. Zapol, P.H. Fuoss, L.A. Curtiss, G.-W. Zhou, J.A. Eastman, Phys. Rev. B 76 (2007) 241404.
[161] W.A. Saidi, M. Lee, L. Li, G.W. Zhou, A.J.H. McGaughey, Phys. Rev. B 86 (2012) 245429.
[162] M.J. Harrison, D.P. Woodruff, J. Robinson, D. Sander, W. Pan, J. Kirschner, Phys. Rev. B 74 (2006) 165402.
[163] K. Tanaka, T. Fujita, Y. Okawa, Surf. Sci. 401 (1998) L407.
[164] K.W. Jacobsen, J.K. Norskov, Phys. Rev. Lett. 65 (1990) 1788.
[165] I. Merrick, J.E. Inglesfield, H. Ishida, Surf. Sci. 551 (2004) 158.
[166] S. Jaatinen, M. Rusanen, P. Salo, Surf. Sci. 601 (2007) 1813.
[167] S. Jaatinen, J. Blomqvist, P. Salo, A. Puisto, M. Alatalo, M. Hirsimaki, M. Ahonen, M. Valden, Phys. Rev. B 75 (2007) 8.
[168] S. Stolbov, T.S. Rahman, J. Chem. Phys. 117 (2002) 8523.
[169] S. Stolbov, T.S. Rahman, Phys. Rev. Lett. 89 (2002) 116101.
[170] S. Stolbov, A. Kara, T.S. Rahman, Phys. Rev. B 66 (2002) 245405.
[171] T. Kangas, K. Laasonen, Surf. Sci. 606 (2012) 192.
[172] M. Lee, A.J.H. McGaughey, Surf. Sci. 604 (2010) 1425.
[173] G.W. Zhou, L. Luo, L. Li, J. Ciston, E.A. Stach, W.A. Saidi, J.C. Yang, Chem. Commun. 49 (2013) 10862.
[174] L.D. Sun, M. Hohage, R. Denk, P. Zeppenfeld, Phys. Rev. B 76 (2007) 245412.

[175] R. Feidenshansl, F. Grey, R.L. Johnson, S.G.J. Mochrie, J. Bohr, M. Nielsen, Phys. Rev. B 41 (1990) 5420.
[176] S.R. Parkin, H.C. Zeng, M.Y. Zhou, K.A.R. Mitchell, Phys. Rev. B 41 (1990) 5432.
[177] L.D. Sun, M. Hohage, P. Zeppenfeld, Phys. Rev. B 69 (2004) 045407.
[178] G. Ertl, Surf. Sci. 6 (1967) 208.
[179] S. Kishimoto, M. Kageshima, Y. Naitoh, Y.J. Li, Y. Sugawara, Surf. Sci. 602 (2008) 2175.
[180] R. Feidenhansl, F. Grey, M. Nielsen, F. Besenbacher, F. Jensen, E. Laegsgaard, I. Stensgaard, K.W. Jacobsen, J.K. Nórskov, R.L. Johnson, Phys. Rev. Lett. 65 (1990) 2027.
[181] D. Coulman, J. Wintterlin, J.V. Barth, G. Ertl, R.J. Behm, Surf. Sci. 240 (1990) 151.
[182] G. Dorenbos, M. Breeman, D.O. Boerma, Phys. Rev. B 47 (1993) 1580.
[183] W. Liu, K.C. Wong, K.A.R. Mitchell, Surf. Sci. 339 (1995) 151.
[184] Q. Liu, L. Li, N. Cai, W.A. Saidi, G.W. Zhou, Surf. Sci. 627 (2014) 75.
[185] A.F. Carley, P.R. Davies, M.W. Roberts, Philos. Trans. R. Soc. A 363 (2005) 829.
[186] D. Coulman, J. Wintterlin, J.V. Barth, G. Ertl, R.J. Behm, Surf. Sci. 240 (1990) 151.
[187] F.M. Chua, Y. Kuk, P.J. Silverman, Phys. Rev. Lett. 63 (1989) 386.
[188] Y. Kuk, F.M. Chua, P.J. Silverman, J.A. Meyer, Phys. Rev. B 41 (1990) 12393.
[189] D. Mocuta, J. Ahner, J.G. Lee, S. Denev, J.T. Yates, Surf. Sci. 436 (1999) 72.
[190] L. Li, N. Cai, W.A. Saidi, G.W. Zhou, Chem. Phys. Lett. 613 (2014) 64.
[191] S.Y. Liem, G. Kresse, J.H.R. Clarke, Surf. Sci. 415 (1998) 194.
[192] K. Kern, H. Niehus, A. Schatz, P. Zeppenfeld, J. George, G. Comsafguif, Phys. Rev. Lett. 67 (1991) 855.
[193] G.W. Zhou, J.C. Yang, Surf. Sci. 531 (2003) 359.
[194] N. Blanchard, D. Martin, P. Weightman, Molecular adsorbate induced restructuring of a stepped Cu(110) surface, in: M. Stutzmann (Ed.), Conferences and Critical Reviews, Phys. Status Solidi C, vol. 2, 2005, p. 4017.
[195] J. Buisset, H.P. Rust, E.K. Schweizer, L. Cramer, A.M. Bradshaw, Surf. Sci. 349 (1996) L147.
[196] P. Zeppenfeld, M. Krzyzowski, C. Romainczyk, G. Comsa, M.G. Lagally, Phys. Rev. Lett. 72 (17) (1994) 2737.
[197] G. Prevot, B. Croset, Y. Girard, A. Coati, Y. Garreau, M. Hohage, L.D. Sun, P. Zeppenfeld, Surf. Sci. 549 (2004) 52.
[198] K. Berge, A. Goldmann, Surf. Sci. 540 (2003) 97.
[199] K. Bobrov, L. Guillemot, Phys. Rev. B 78 (2008) 121408.
[200] J. Harl, G. Kresse, Surf. Sci. 600 (2006) 4633.
[201] L. Guillemot, K. Bobrov, Phys. Rev. B 83 (2011) 075409.
[202] D. Vanderbilt, Surf. Sci. 268 (1992) L300.
[203] F. Frechard, R.A. van Santen, Surf. Sci. 407 (1998) 200.
[204] J. Bamidele, J. Brndiar, A. Gulans, L. Kantorovich, I. Stich, J. Chem. Theory Comput. 9 (2013) 5578.
[205] J. Klimes, A. Michaelides, J. Chem. Phys. 137 (2012) 120901.
[206] L. Schimka, J. Harl, A. Stroppa, A. Grüneis, M. Marsman, F. Mittendorfer, G. Kresse, Nat. Mater. 9 (2010) 741.
[207] J. Carrasco, A. Hodgson, A. Michaelides, Nat. Mater. 11 (2012) 667.
[208] R.A. Didio, D.M. Zehner, E.W. Plummer, J. Vac. Sci. Technol. A 2 (1984) 852.
[209] P. Cortona, C. Sapet, Surf. Sci. 585 (2005) 155.
[210] R. Courths, B. Cord, H. Wern, H. Saalfeld, S. Hufner, Solid State Commun. 63 (1987) 619.
[211] R. Matzdorf, A. Goldmann, Surf. Sci. 412 (1998) 61.
[212] P. Cabrera-Sanfelix, C. Lin, A. Arnau, D. Sanchez-Portal, J. Phys. Condens. Matter 25 (2013) 135003.
[213] F. Pforte, A. Gerlach, A. Goldmann, R. Matzdorf, J. Braun, A. Postnikov, Phys. Rev. B 63 (2001) 165405.
[214] L. Li, G.W. Zhou, Surf. Sci. 615 (2013) 57.
[215] J. Li, L. Li, G. Zhou, J. Chem. Phys. 142 (2015) 084701.
[216] G.W. Simmons, D.F. Mitchell, K.R. Lawless, Surf. Sci. 8 (1967) 130.
[217] J.H. Ho, R.W. Vook, J. Cryst. Growth 44 (1978) 561.
[218] H. Niehus, Surf. Sci. 130 (1983) 41.
[219] J. Haase, H.J. Kuhr, Surf. Sci. 203 (1988) L695.
[220] B. Luo, J. Urban, J. Phys. Condens. Matter 3 (1991) 2873.
[221] F. Jensen, F. Besenbacher, E. Laegsgaard, I. Stensgaard, Surf. Sci. 259 (1991) L774.
[222] W.E.J. Vankooten, O.L.J. Gijzeman, J.W. Geus, Surf. Sci. 280 (1993) L243.
[223] T. Matsumoto, R.A. Bennett, P. Stone, T. Yamada, K. Domen, M. Bowker, Surf. Sci. 471 (2001) 225.
[224] F. Wiame, V. Maurice, P. Marcus, Surf. Sci. 601 (2007) 1193.
[225] W. Jacob, V. Dose, A. Goldmann, Appl. Phys. A 41 (1986) 145.
[226] L.C. Ma, J.M. Zhang, K.W. Xu, Sci. China—Phys. Mech. Astron. 56 (2013) 573.
[227] X.-Y. Pang, L.-Q. Xue, G.-C. Wang, Langmuir 23 (2007) 4910.
[228] R.W. Judd, P. Hollins, J. Pritchard, Surf. Sci. 171 (1986) 643.
[229] R.L. Toomes, D.P. Woodruff, M. Polcik, S. Bao, P. Hofmann, K.M. Schindler, Surf. Sci. 445 (2000) 300.
[230] K. Moritani, M. Okada, Y. Teraoka, A. Yoshigoe, T. Kasai, J. Phys. Chem. C 112 (2008) 8662.
[231] N.A. Richter, C.-E. Kim, C. Stampfl, A. Soon, Phys. Chem. Chem. Phys. 16 (2014) 26735.
[232] A. Michaelides, K. Reuter, M. Scheffler, J. Vac. Sci. Technol. A 23 (2005) 1487.
[233] J. Schnadt, A. Michaelides, J. Knudsen, R.T. Vang, K. Reuter, E. Lægsgaard, M. Scheffler, F. Besenbacher, Phys. Rev. Lett. 96 (2006) 146101.
[234] A. Michaelides, M.L. Bocquet, P. Sautet, A. Alavi, D.A. King, Chem. Phys. Lett. 367 (2003) 344.
[235] M.L. Bocquet, A. Michaelides, P. Sautet, D.A. King, Phys. Rev. B 68 (2003) 075413.
[236] M. Todorova, K. Reuter, M. Scheffler, J. Phys. Chem. B 108 (2004) 14477.
[237] C. Stampfl, Catal. Today 105 (2005) 17.
[238] J. Gustafson, A. Mikkelsen, M. Borg, E. Lundgren, L. Kohler, G. Kresse, M. Schmid, P. Varga, J. Yuhara, X. Torrelles, C. Quiros, J.N. Andersen, Phys. Rev. Lett. 92 (2004) 126102.
[239] L. Kohler, G. Kresse, M. Schmid, E. Lundgren, J. Gustafson, A. Mikkelsen, M. Borg, J. Yuhara, J.N. Andersen, M. Marsman, P. Varga, Phys. Rev. Lett. 93 (2004) 266103.
[240] M. Todorova, K. Reuter, M. Scheffler, Phys. Rev. B 71 (2005) 195403.
[241] J.A. Eastman, P.H. Fuoss, L.E. Rehn, P.M. Baldo, G.W. Zhou, D. D. Fong, L.J. Thompson, Appl. Phys. Lett. 87 (2005) 051914.
[242] J.F. Pierson, D. Wiederkehr, A. Billard, Thin Solid Films 478 (2005) 196.
[243] D.A. Goulden, Philos. Mag. 33 (1976) 393.
[244] F.W. Young, J.V. Cathcart, A.T. Gwathmey, Acta Metall. 4 (1956) 145.
[245] A.T. Gwathmey, A.F. Benton, J. Phys. Chem. 46 (1942) 969.
[246] T.N. Rhodin, J. Am. Chem. Soc. 72 (1950) 5102.
[247] L.O. Brockway, I.M. Adler, J. Electrochem. Soc. 119 (1972) 899.
[248] R.H. Milne, A. Howie, Philos. Mag. A 49 (1984) 665.
[249] J.C. Yang, M. Yeadon, B. Kolasa, J.M. Gibson, Appl. Phys. Lett. 70 (1997) 3522.
[250] J.C. Yang, M. Yeadon, B. Kolasa, J.M. Gibson, Scr. Mater. 38 (1998) 1237.
[251] P. Stefanov, T. Marinova, Appl. Surf. Sci. 31 (1988) 445.
[252] L. Luo, Y. Kang, J.C. Yang, G. Zhou, Surf. Sci. 606 (2012) 1790.
[253] G.W. Zhou, Acta Mater. 57 (2009) 4432.
[254] G.W. Zhou, J.C. Yang, Appl. Surf. Sci. 210 (2003) 165.
[255] G.W. Zhou, W.S. Slaughter, J.C. Yang, Phys. Rev. Lett. 94 (2005) 246101.
[256] G. Zhou, J. Appl. Phys. 105 (2009) 104302.
[257] J. Tersoff, R.M. Tromp, Phys. Rev. Lett. 70 (1993) 2782.
[258] M. Lampimaki, K. Lahtonen, M. Hirsimaki, M. Valden, J. Chem. Phys. 126 (2007) 034703.
[259] J.C. Yang, M.D. Bharadwaj, G.W. Zhou, L. Tropia, Microsc. Microanal. 7 (2001) 486.
[260] X. Bao, M. Muhler, B. Pettinger, Y. Uchida, G. Lehmpfuhl, R. Schlogl, G. Ertl, Catal. Lett. 32 (1995) 171.
[261] A. Bottcher, H. Niehus, J. Chem. Phys. 110 (6) (1999) 3186.
[262] T. Kangas, K. Laasonen, Surf. Sci. 602 (2008) 3239.

[263] T. Kangas, K. Laasonen, A. Puisto, H. Pitkanen, M. Alatalo, Surf. Sci. 584 (2005) 62.
[264] M.Y. Lee, J.H. McGaughey, Surf. Sci. 603 (2009) 3404.
[265] M. Alatalo, A. Puisto, H. Pitkanen, A.S. Foster, K. Laasonen, Surf. Sci. 600 (2006) 1574.
[266] M. Ahonen, M. Hirsimaki, A. Puisto, S. Auvinen, M. Valden, M. Alatalo, Chem. Phys. Lett. 456 (2008) 211.
[267] P. Junell, M. Ahonen, M. Hirsimaki, M. Valden, Surf. Rev. Lett. 11 (2004) 457.
[268] B. Devine, T.R. Shan, Y.T. Cheng, A.J. McGaughey, M.Y. Lee, S. Phillpot, S.B. Sinnot, Phys. Rev. B 84 (2011) 125308.
[269] A. Laio, M. Parrinello, Proc. Natl Acad. Sci. 99 (2002) 12562.
[270] J.C. Yang, B. Kolasa, J.M. Gibson, M. Yeadon, Appl. Phys. Lett. 73 (1998) 2841.
[271] J.C. Yang, M. Yeadon, B. Kolasa, J.M. Gibson, J. Electrochem. Soc. 146 (1999) 2103.
[272] G.W. Zhou, L. Wang, J.C. Yang, J. Appl. Phys. 97 (2005) 063509.
[273] G.W. Zhou, J.C. Yang, J. Mater. Res. 20 (2005) 1684.
[274] L. Li, L. Luo, J. Ciston, W.A. Saidi, E.A. Stach, J.C. Yang, G. Zhou, Phys. Rev. Lett. 113 (2014) 136104.
[275] G.W. Zhou, J.C. Yang, Appl. Surf. Sci. 222 (2004) 357.
[276] G.W. Zhou, J.C. Yang, Surf. Sci. 559 (2004) 100.
[277] G.W. Zhou, J.C. Yang, Phys. Rev. Lett. 89 (2002) 4.
[278] G.W. Zhou, Appl. Phys. Lett. 94 (2009) 233115.
[279] G.W. Zhou, X.D. Chen, D. Gallagher, J.C. Yang, Appl. Phys. Lett. 93 (2008) 3.
[280] K.R. Lawless, A.T. Gwathmey, Acta Metall. 4 (1956) 153.
[281] M. Rauh, P. Wissmann, Thin Solid Films 228 (1993) 121.
[282] F.M. Ross, J.M. Gibson, Phys. Rev. Lett. 68 (1992) 1782.
[283] G. Dujardin, A. Mayne, G. Comtet, L. Hellner, M. Jamet, E. LeGoff, P. Millet, Phys. Rev. Lett. 76 (1996) 3782.
[284] K. Thurmer, E. Williams, J. Reutt-Robey, Science 297 (2002) 2033.
[285] G. Dujardin, A.J. Mayne, F. Rose, Phys. Rev. Lett. 82 (1999) 3448.
[286] A.J. Mayne, F. Rose, G. Dujardin, Surf. Sci. 523 (2003) 157.
[287] M. Okada, L. Vattuone, A. Gerbi, L. Savio, M. Rocca, K. Moritani, Y. Teraoka, T. Kasai, J. Phys. Chem. C 111 (2007) 17340.
[288] Q. Zhu, W.A. Saidi, J.C. Yang, J. Phys. Chem. C 119 (2015) 251.
[289] P.A. Mulheran, J.A. Blackman, Philos. Mag. Lett. 72 (1995) 55.
[290] M.C. Bartelt, J.W. Evans, Phys. Rev. B 54 (1996) R17359.
[291] W.H. Orr, J. Electrochem. Soc. 111 (1964) C184.
[292] P.H. Holloway, J.B. Hudson, Surf. Sci. 43 (1974) 123.
[293] A.N. Kolmogorov, Bull. Acad. Sci. USSR 3 (1937) 355.
[294] M. Avrami, J. Chem. Phys. 7 (1939) 1103.
[295] W.A. Johnson, R.F. Mehl, Trans. Am. Inst. Min. Metall. Eng. 135 (1939) 416.
[296] B. Jeon, S.K.R.S. Sankaranarayanan, A.C.T. van Duin, S. Ramanathan, Philos. Mag. 91 (2011) 4073.
[297] H. Leidheiser, The Corrosion of Copper, Tin, and their Alloys, Corrosion Monograph Series, Wiley, New York, 1971.
[298] A. Ronnquist, H. Fischmeister, J. Inst. Met. 89 (1960) 65.
[299] T.N. Rhodin, J. Am. Chem. Soc. 73 (1951) 3143.
[300] L. Bouzidi, A.J. Slavin, Surf. Sci. 580 (2005) 195.
[301] J.W. Lim, Y. Ishikawa, K. Miyake, M. Yamashita, M. Isshiki, Mater. Trans. 43 (2002) 1403.
[302] P.T. Landsberg, J. Chem. Phys. 23 (1955) 1079.
[303] T.B. Grimley, B.M.W. Trapnell, Proc. R. Soc. A 234 (1956) 405.
[304] H.H. Uhlig, Acta Metall. 4 (1956) 541.
[305] U.R. Evans, Trans. Electrochem Soc. 91 (1947) 547.
[306] N. Cabrera, N.F. Mott, Rep. Prog. Phys. 12 (1948) 163.
[307] Y.Z. Hu, R. Sharangpani, S.P. Tay, J. Vac. Sci. Technol. A 18 (2000) 2527.
[308] S.K. Roy, S.C. Sircar, Oxid. Met. 15 (1981) 9.
[309] H. Derin, K. Kantarli, Appl. Phys. A 75 (2002) 391.
[310] R. van Wijk, O.L.J. Gijzeman, J.W. Geus, Appl. Surf. Sci. 93 (1996) 237.
[311] A. Njeh, T. Wieder, H. Fuess, Surf. Interface Anal. 33 (2002) 626.
[312] A. Manara, V. Sirtori, L. Mammarella, Surf. Interface Anal. 18 (1992) 32.
[313] E.G.J. Clarke, A.W. Czanderna, Surf. Sci. 49 (1975) 529.
[314] K. Fujita, D. Ando, M. Uchikoshi, K. Mimura, M. Isshiki, Appl. Surf. Sci. 276 (2013) 347.
[315] M. O'Reilly, X. Jiang, J.T. Beechinor, S. Lynch, C.N. Nidheasuna, J. C. Patterson, G.M. Crean, Appl. Surf. Sci. 91 (1995) 152.
[316] W. Gao, H. Gong, J. He, A. Thomas, L. Chan, S. Li, Mater. Lett. 51 (2001) 78.
[317] P. Keil, R. Frahm, D. Lutzenkirchen-Hecht, Corros. Sci. 52 (2010) 1305.
[318] P. Keil, D. Lutzenkirchen-Hecht, R. Frahm, Investigation of room temperature oxidation of Cu in air by Yoneda-XAFS, in: 13th International Conference on X-Ray Absorption Fine Structure (XAFS13), Aip Conference Proceedings, vol. 882, American Institute of Physics, Melville, 2007, p. 490.
[319] Z.-J. Zuo, J. Li, P.-D. Han, W. Huang, J. Phys. Chem. C 118 (2014) 20332.
[320] S.K. Chawla, B.I. Rickett, N. Sankarraman, J.H. Payer, Corros. Sci. 33 (1992) 1617.
[321] Y.S. Chu, I.K. Robinson, A.A. Gewirth, J. Chem. Phys. 110 (1999) 5952.
[322] S. Suzuki, Y. Ishikawa, M. Isshiki, Y. Waseda, Mater. Trans. JIM 38 (1997) 1004.
[323] V. Rico, A. Borrás, F. Yubero, J.P. Espinós, F. Frutos, A.R. González-Elipe, J. Phys. Chem. C 113 (2009) 3775.
[324] I. Platzman, C. Saguy, R. Brener, R. Tannenbaum, H. Haick, Langmuir 26 (2010) 191.
[325] S. Yamamoto, H. Bluhm, K. Andersson, G. Ketteler, H. Ogasawara, M. Salmeron, A. Nilsson, J. Phys. Condens. Matter 20 (2008) 14.
[326] K. Chen, S. Song, D. Xue, Cryst. Eng. Commun. 15 (2013) 144.
[327] Y.F. Zhu, K. Mimura, J.W. Lim, M. Isshiki, Q. Jiang, Metall. Mater. Trans. A 37A (2006) 1231.
[328] V.V. Belousov, A.A. Klimashin, Russ. Chem. Rev. 82 (2013) 273.
[329] J.E. Boggio, J. Chem. Phys. 70 (1979) 5054.
[330] R. Courths, S. Hufner, P. Kemkes, G. Wiesen, Surf. Sci. 376 (1997) 43.
[331] T. Schimizu, M. Tsukada, Surf. Sci. 295 (1993) L1017.
[332] M. Todorova, W.X. Li, M.V. Ganduglia-Pirovano, C. Stampfl, K. Reuter, M. Scheffler, Phys. Rev. Lett. 89 (2002) 096103.
[333] M. Forster, R. Raval, J. Carrasco, A. Michaelides, A. Hodgson, Chem. Sci. 3 (2012) 93.
[334] C.X. Kronawitter, C. Riplinger, X.B. He, P. Zahl, E.A. Carter, P. Sutter, B.E. Koel, J. Am. Chem. Soc. 136 (2014) 13283.
[335] X.Y. Deng, A. Verdaguer, T. Herranz, C. Weis, H. Bluhm, M. Salmeron, Langmuir 24 (2008) 9474.
[336] P. Jiang, J.L. Chen, F. Borondics, P.A. Glans, M.W. West, C.L. Chang, M. Salmeron, J.H. Guo, Electrochem. Commun. 12 (2010) 820.
[337] M. DellAngela, T. Anniyev, M. Beye, R. Coffee, A. Foehlisch, J. Gladh, T. Katayama, S. Kaya, O. Krupin, J. LaRue, A. Møgelhøj, D. Nordlund, J.K. Nørskov, H. Öberg, H. Ogasawara, H. ÖstrÖm, L.G.M. Pettersson, W.F. Schlotter, J.A. Sellberg, F. Sorgenfrei, J.J. Turner, M. Wolf, W. Wurth, A. Nilsson, Science 339 (2013) 1302.
[338] J. Schnadt, J. Knudsen, J.N. Andersen, H. Siegbahn, A. Pietzsch, F. Hennies, N. Johansson, N. Mårtensson, G. Öhrwall, S. Bahr, S. Mähl, O. Schaff, J. Synchrotron Radiat. 19 (2012) 701.
[339] H. Bluhm, J. Electron Spectrosc. 177 (2010) 71.
[340] C.T. Herbschleb, P.C. van der Tuijn, S.B. Roobol, V. Navarro, J.W. Bakker, Q. Liu, D. Stoltz, M.E. Cañas-Ventura, G. Verdoes, M.A. van Spronsen, M. Bergman, L. Crama, I. Taminiau, A. Ofitserov, G.J.C. van Baarle, J.W.M. Frenken, Rev. Sci. Instrum. 85 (2014) 083703.
[341] M. Rossler, P. Geng, J. Wintterlin, Rev. Sci. Instrum. 76 (2005) 023705.
[342] L. Liu, A. Laio, A. Michaelides, Phys. Chem. Chem. Phys. 13 (2011) 13162.